Green Chemistry

PAPER

View Article Online
View Journal



Cite this: DOI: 10.1039/d6gc01907b

# Upcycling waste PET into functional multiblock copolymers through controlled macromolecular design

Shelby Watson-Sanders, [a] Alison Biery, [a] Karina Guerrero,[a] Nicholas J. Galan, [b] Tomonori Saito, [b] Brian K. Long [a] and Mark D. Dadmun *[a]

Poly(ethylene terephthalate) (PET) oligomers derived from glycolysis depolymerization were converted into multiblock copolymers through diisocyanate-mediated coupling with dihydroxy-terminated oligomers, enabling precise control over copolymer sequence distribution, connectivity, and mechanical performance. Here, we demonstrate that telechelic PET oligomers isolated directly from depolymerized consumer waste can serve as reactive building blocks for the formation of segmented multiblock copolymers, eliminating the need to revert to monomeric feedstocks. Dihydroxy-terminated PET oligomers ($M_w \approx 8$ kg mol$^{-1}$) were coupled with poly(ethylene oxide) (PEO, $M_w \approx 4$ kg mol$^{-1}$) to form PET-PEO multiblock copolymers with high molar mass ($M_w \approx 160$ kg mol$^{-1}$). We further show that the timing of end-capping reactions provides a key control parameter that governs the competition between chain extension and termination, thereby dictating the resulting multiblock architecture and molecular-weight evolution. Evaluation of their mechanical properties reveals that virgin PET exhibits high modulus (~3 GPa) and strength (43 MPa) but limited ductility (<10% elongation). In contrast, PET–PEO multiblock copolymers retain comparable tensile strength (44 MPa), albeit while exhibiting dramatically enhanced ductility (>90% elongation), forming tougher materials with efficient stress transfer between the rigid PET domains and the flexible PEO segments. When incorporated into PET/PEO blends at low loadings, the multiblock copolymers serve as effective compatibilizers, yielding materials with an intermediate modulus (1.1–1.2 GPa) and improved elongation compared to uncompatibilized blends. Furthermore, the presence of PEO blocks increases water uptake and gas permeability relative to virgin PET, reflecting the tunability of molecular transport through the copolymeric blocks. To our knowledge, this represents the first report of PET–PEO multiblock copolymers derived from post-consumer PET for gas transport applications. These results demonstrate that multiblock copolymer formation from telechelic PET oligomers provides a versatile platform for tailoring the mechanical and transport behavior of polyester-based materials through controlled macromolecular design and establishes a generalizable strategy for transforming consumer plastic waste into functional segmented polymers without requiring complete depolymerization to monomers.

Received 30th March 2026,
Accepted 12th May 2026

DOI: 10.1039/d6gc01907b

rsc.li/greenchem



## Green foundation

1. This work advances green chemistry forward by developing a method to upcycle PET waste into functional multiblock copolymers through the interception of telechelic oligomers, eliminating the need for complete depolymerization into monomers and allows direct conversion of waste into architecturally controlled materials.
2. Depolymerized PET is transformed into high-molecular-weight ($M_w \approx 160$ kg mol$^{-1}$) multiblock copolymers that feature improved ductility (>90% elongation) and adjustable gas transport properties. The end-capping time is used as a control parameter to tailor polymer architecture from waste-derived intermediates.
3. Future efforts will focus on PET textile waste to tackle dye-contaminated streams, replace diisocyanates with more environmentally friendly coupling chemistries, and incorporate both blocks from recycled feedstocks to create fully waste-derived multiblock materials.

## Introduction

Global plastic production has increased exponentially since the mid-20th century, exceeding 400 million metric tons

[a]Department of Chemistry, University of Tennessee, Knoxville, TN 37996, USA. E-mail: Dad@utk.edu
[b]Oak Ridge National Laboratory, Oak Ridge, TN, USA

annually and projected to approach 900 million metric tons per year within the next three decades.[1–6] Despite advances in waste management, an estimated 10–15 million metric tons of plastic enter the environment each year, driven by improper disposal, runoff, and industrial discharge.[7–12] The persistence of plastics has resulted in widespread ecological impacts, including the accumulation of micro- and nanoplastics across marine and terrestrial ecosystems.[9–12] Without substantial intervention, both plastic production and environmental leakage are expected to increase markedly by mid-century.[5–13] These challenges underscore the urgent need for strategies that not only recycle plastics but also enable their transformation into higher-value materials.

The limitations of current polymer recycling strategies exacerbate this challenge. Mechanical recycling, while economically attractive, often results in polymer degradation, downcycling, and variable material properties due to contamination and processing history.[1,14–17] It is also imperfect at sorting, and incompatibility between polymers results in brittle, macrophase-separated blends with weak interfaces, limiting their usefulness in most applications.[18–20] Energy recovery approaches, including incineration and pyrolysis, permanently remove material from the circular economy and generate greenhouse gas emissions.[21–29] Chemical recycling enables depolymerization into monomers or oligomers; however, industrial processes such as PET glycolysis remain challenged by slow kinetics, cyclic oligomer formation, and higher costs relative to virgin materials.[1,14–17] Consequently, less than 10% of all plastics produced to date are recycled, while the majority are landfilled or incinerated.[3,4] Importantly, most chemical recycling strategies focus on recovering monomeric species, which limits the ability to directly access advanced polymer architectures from waste-derived intermediates.

Poly(ethylene terephthalate) (PET), one of the most widely produced commodity polymers, has emerged as a key target for advanced recycling strategies. Our group previously demonstrated that PET oligomers obtained from glycolysis undergo solid-state polymerization (SSP), wherein hydroxyl end groups react with ester linkages along the polymer backbone to increase molar mass.[30] This process preferentially extends higher-molecular-weight chains, resulting in larger increases in weight-average molar mass ($M_w$) than in number-average molar mass ($M_n$), consistent with trends observed during conventional PET polycondensation.[15,30] While effective for molar mass recovery, such approaches remain limited to closed-loop recycling. Thus, new strategies are needed to move beyond molar mass restoration and toward the creation of new polymer architectures from PET-derived intermediates.

In contrast, chemical upcycling seeks to transform waste polymers into new materials with tailored or enhanced functionality, rather than regenerating the original polymer.[31] Recent studies demonstrate that PET-derived monomers and oligomers can serve as versatile building blocks for polyurethanes, epoxy networks, and functional copolymers, enabling diversification of properties and value enhancement beyond the constraints of closed-loop recycling.[31–45] These advances leverage improved catalyst design and process control to repurpose polymer-derived carbon into higher-performance materials. In parallel, emerging work on covalent adaptable networks (CANs) highlights how dynamic covalent linkages and oligomeric building blocks can be leveraged to create recyclable, value-added polymer networks, suggesting a promising framework for similarly converting PET-derived oligomers into high-performance materials.[46,47] However, these approaches typically rely on fully depolymerized monomers or broadly distributed oligomer mixtures, and do not exploit isolated, well-defined telechelic intermediates as controllable macromolecular building blocks.

A particularly promising strategy within this framework is the interception of depolymerization intermediates as telechelic macromers, enabling their incorporation into new polymer architectures as feedstocks. Building on our prior isolation of dihydroxy-terminated PET oligomers directly from glycolysis,[30,48] we propose that these telechelic oligomers can serve as programmable building blocks for the synthesis of segmented multiblock copolymers without requiring conversion back to monomeric species. To our knowledge, the use of waste-derived PET telechelic oligomers as controlled precursors for the formation of multiblock copolymers has not been previously demonstrated. The present work explores both repolymerization and upcycling of PET telechelic oligomers into novel multiblock copolymers *via* diisocyanate coupling. Using PET-derived oligomers and monomers as feedstocks, we synthesize new polymer architectures and evaluate their mechanical properties, water swelling behavior, and permeation characteristics. This approach establishes a direct pathway from consumer waste to architecturally controlled polymer systems.

In this work, we report a strategy for converting depolymerized PET into PET–PEO multiblock copolymers through hexamethylene diisocyanate (HDI)-mediated end-capping and subsequent polyether incorporation. We hypothesize that the timing of the end-capping step governs the competition between chain extension and termination, providing a key control parameter over multiblock architecture formation. Rather than prescribing a fixed block sequence, we demonstrate that the effective PET–PEO architecture arises from the duration of the end-capping step, which governs the extent of intermolecular coupling before PEO incorporation. This architectural variability has profound consequences for phase behavior, mechanical response, water uptake, and gas transport properties. While segmented poly(ether–ester) systems such as PBT–PEO have been widely studied for gas separation membranes, PET–PEO multiblock systems—particularly those derived from post-consumer waste—remain unexplored. By comparing these multiblock materials with virgin PET, repolymerized PET (rPET), phase-separated PET/PEO blends, and literature poly(ether–ester) membranes, we establish end-capping time as a powerful, experimentally accessible handle for tuning the performance of upcycled PET-based materials. More broadly, this work demonstrates how consumer PET waste can be transformed into functional, membrane-relevant materials without reverting to monomer feedstocks.

 

# Methods

### Materials preparation

PET was sourced from commercial soda bottles, which were washed and cut into squares (8 mm × 5 mm × 0.3 mm). 1,5,7-Triazabicyclo[4.4.0]dec-5-ene (98.0+%, TCI America™), methanesulfonic Acid (99%), ethylene glycol, (99.8%, anhydrous, AcroSeal™, Thermo Scientific Chemicals), tetrahydrofuran (THF), bis(2-hydroxyethyl) terephthalate (85.0+%, TCI America™), 1,1,2,2-tetrachloroethane (TCE), methanol, 20 mL vials, 100 mL round bottom flasks, 12.7 × 8 mm stir bars, and 12 × 4.5 mm stir bars were sourced from Fischer Scientific. Hexamethylene diisocyanate and 4 kg mol$^{-1}$ polyethylene oxide (PEO) were sourced from Sigma-Aldrich (formerly Millipore Sigma). All chemicals were used as received.

### BHET polymerization *via* excess diisocyanate coupling

A 50 mL round-bottom flask was charged with dihydroxy-capped bis(2-hydroxyethyl) terephthalate (BHET)(1 g), a stir bar, and then sealed with a septum. The round-bottom flask was flushed with $N_2$ gas, and then 10 mL of tetrachloroethane (TCE) was added. The vessel was placed in a 130 °C oil bath on a 250 RPM stir plate to allow the BHET to dissolve in the TCE. Once the BHET was fully dissolved, 1,6-diisocyanatohexane (HDI) was added in a 1 : 1 molar ratio of isocyanate to hydroxyl end groups (HDI/PEO), as shown in Scheme 1. Aliquots were taken at 0.25, 0.5, 1, and 2 h, respectively. After stirring for 18 h, the reaction was quenched and precipitated with a 250 mL mixture of 1 : 10 isopropyl alcohol (IPA):hexane. IPA was utilized to terminate the reaction to react with any residual isocyanate groups.

### PEO repolymerization *via* excess diisocyanate coupling

A 50 mL round-bottom flask was charged with dihydroxy-capped polyethylene oxide (PEO, 1 g, 4 kg mol$^{-1}$ $M_n$, 1.06 $Đ$), a stir bar, and then sealed with a septum. The round-bottom flask was flushed with $N_2$ gas, and then 10 mL of TCE was added. The vessel was placed in an oil bath at 130 °C on a 250 RPM stir plate to allow the PEO to dissolve in the TCE. Once the PEO was fully dissolved, HDI was added in a 1 : 1 molar ratio of isocyanate to hydroxyl end groups (HDI/PEO), as shown in Scheme 2. Aliquots were taken at 0.25, 0.5, 1, and 2 h, respectively. After stirring for a total of 24 h, the reaction was quenched and precipitated with a 250 mL mixture of 1 : 10 isopropyl alcohol (IPA):hexane. IPA was utilized to terminate the reaction by reacting with any residual isocyanate groups.

### PET repolymerization *via* diisocyanate coupling

A 50 mL round-bottom flask was charged with dihydroxy-capped (1.7 hydroxyl groups per chain on average) polyethylene terephthalate (PET, 1 g, 28 kDa $M_v$) and a stir bar, and then sealed with a septum. The round-bottom flask was flushed with $N_2$ gas, and then 10 mL of TCE was added. The vessel was placed in a 140 °C oil bath on a 250 RPM stir plate to allow the PET to dissolve in the TCE. Once the PET was fully dissolved, HDI was added in a 1 : 1 or 2 : 1 molar ratio of isocyanate to hydroxyl end groups (HDI/PEO), as shown in Scheme S5. After the reaction ran for 24 hours, it was quenched with a 250 mL mixture of 1 : 10 isopropyl alcohol (IPA):hexane. PET is insoluble in hexane, allowing for the polymer to precipitate. IPA was utilized to terminate the reaction by reacting with any residual isocyanate groups.

### Multiblock copolymer (MBCP) PET-PEO: 10 min end-capping

Prior to HDI-mediated coupling, the depolymerized PET oligomers were purified to remove residual TBD : MSA catalyst and ethylene glycol. The solid glycolysis product was dissolved in HFIP and precipitated into methanol, collected, and dried; this HFIP/MeOH dissolution–precipitation protocol was repeated three times. These repeated precipitations remove low-molecular-weight species, including the TBD : MSA salt and residual EG, yielding a purified telechelic PET oligomer fraction that was used as the feedstock for subsequent PET–PEO multiblock synthesis.

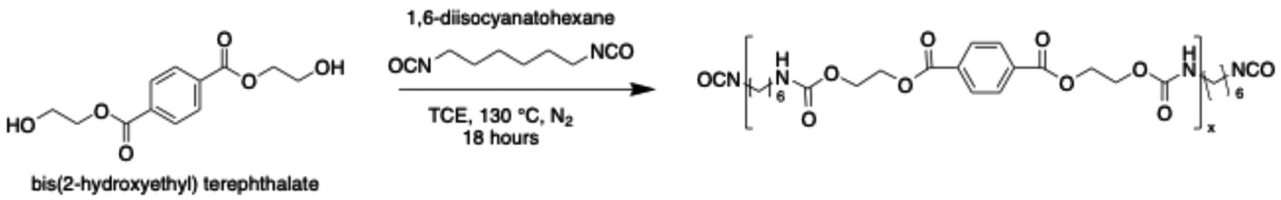


Scheme 1 Polymerization of bis(2-hydroxyethyl) terephthalate (BHET) oligomer with 1,6-diisocyanatohexane (HDI).

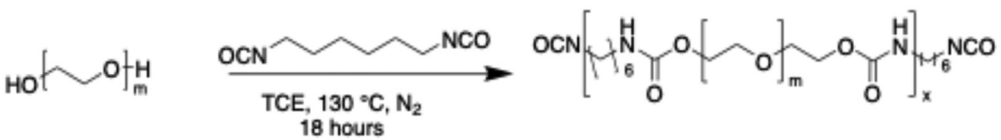


Scheme 2 Polymerization of polyethylene oxide (PEO) oligomer with 1,6-diisocyanatohexane (HDI).

A 50 mL round-bottom flask was charged with dihydroxy-capped PET oligomers (1 g, $M_n$ = 5.5 kg mol$^{-1}$, $Đ$ = 1.88) and a stir bar, and then sealed with a septum. The round-bottom flask was flushed with $N_2$ gas, and then 10 mL of TCE was added. The vessel was placed in a 140 °C oil bath on a 250 RPM stir plate to allow the PET to dissolve in the TCE. Once the PET was fully dissolved, the oil bath temperature was decreased to 130 °C, and HDI was added in a 2.05 : 1 molar ratio of isocyanate to hydroxyl end groups (HDI/PET), as shown in Scheme 3. The coupling reactions were conducted at 130 °C, which we identified as the lowest temperature at which PET oligomers remain fully dissolved in TCE and the reaction mixture stays homogeneous over the required timescales. Because lower temperatures lead to PET precipitation and heterogeneous mixtures, the reaction temperature was held fixed at 130 °C, and the end-capping time was systematically varied as the primary parameter controlling multiblock architecture (see methods section of SI).

A 10 wt% mixture of PEO (4 kg mol$^{-1}$, 1.06 $Đ$) in TCE flushed with $N_2$ gas was made. Once the diisocyanate coupling reaction of PET had run for 10 min, PEO dissolved in TCE was added in a 1 : 1 molar ratio of PEO hydroxyl groups to PET hydroxyl groups, as shown in Scheme 4. After the reaction ran for a total of 22 h, the reaction was quenched and precipitated with a 250 mL mixture of 1 : 10 isopropyl alcohol (IPA) : hexane. For PET–PEO multiblock synthesis, PET oligomers, HDI, and PEO were reacted in a single pot without isolating the PET–HDI intermediate. HDI was added in a 2.05 : 1 molar ratio relative to PET hydroxyl groups to provide sufficient isocyanate functionality to end-cap both PET chain ends, to allow subsequent coupling to PEO. After the desired total reaction time, the PET–HDI and PEO reaction mixture was quenched with isopropanol (IPA) to react with any residual isocyanate groups, thereby terminating chain growth and preventing further formation of PEO–HDI species.

### Size exclusion chromatography (SEC)

Size-exclusion chromatography was used to analyze the molecular-weight characteristics of depolymerization and repolymerization products over time. The GPC analyses for PEO and BHET–PEO were carried out using a THF-based Gel Permeation Chromatograph/Size Exclusion Chromatograph (GPC/SEC). The system employed a Tosoh EcoSEC GPC with a refractive index (RI) detector, calibrated to polystyrene standards from 600 Da to 2230 kg mol$^{-1}$. The column setup included two Tosoh TSKgel SuperMultiporeHZ-M columns (4.6 × 150 mm and 4 m) and a guard column. Samples were run at 0.35 mL min$^{-1}$ and analyzed at 40 °C. Prior to analysis, samples were dissolved overnight in THF at 1.5 mg mL$^{-1}$, filtered through a 0.2 μm PTFE filter, and loaded into the autosampler. For PET and PET-PEO, GPC analyses were performed in 1,1,1,3,3,3-hexafluoroisopropanol (HFIP) using a GPC/SEC system. Samples were dissolved in HFIP for five days, filtered into an autosampler vial, and analyzed on an Agilent 1260 Infinity II LC with a Guard column (PL Gel 5 μm, 50 × 4.6 mm) and two PL HFIP gel columns (250 × 4.6 mm, 9 μm). The mobile phase was HFIP at 0.3 mL min$^{-1}$. Calibration used an Agilent EasiVial PMMA standard containing four molar masses. Detection involved a differential RI detector and a multi-angle light scattering detector at 90° and 15°. Molar masses ($M_n$ and $M_w$) and dispersity ($Đ = M_w/M_n$) were calculated based on system calibration, assuming full mass elution from columns, using the Agilent GPC/SEC software.

### Intrinsic viscosity molar mass, $M_v$

The viscosity average molar mass of the depolymerization products is monitored using a Schott instrument Kapillarviskosimetr 531-10. In this experiment, the PET samples (90–100 mg) were dissolved in HFIP (15 mL) for five days before their intrinsic viscosity (IV) was measured. The samples were equilibrated in the viscometer at 25 °C for

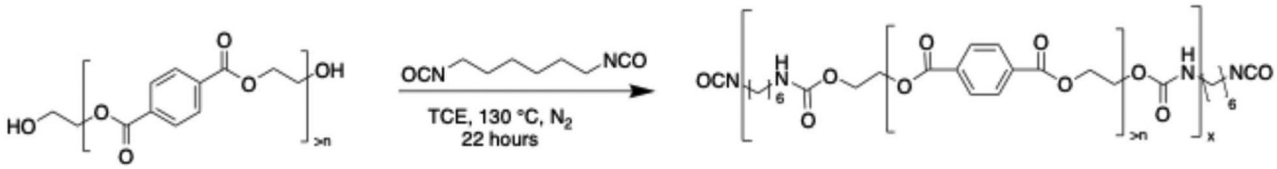


**Scheme 3** Polymerization of polyethylene terephthalate (PET) with 1,6-diisocyanatohexane (HDI).

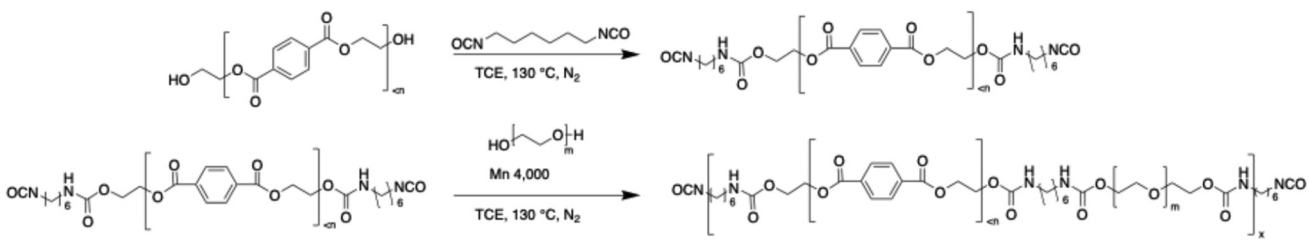


**Scheme 4** End-capping of PET oligomer with 1,6-diisocyanatohexane (HDI) and then polymerization of PEO oligomer with diisocyanate-PET macromonomer.

5 minutes before the viscosity was measured. The concentration dependence of the flow times of the PET solution through the viscometer was measured in quadruplicate at each concentration. After four trial times were gathered, the sample was diluted, equilibrated, and run again to obtain the concentration dependence of the flow times. The reduced and inherent viscosities of the PET solutions at each concentration were determined from the measured flow times using eqn (1)–(5). Intrinsic viscosity was determined by finding the *y*-intercept of the plots of reduced and inherent viscosity as a function of concentration. The viscosity average molar mass ($M_v$) of the PET was then determined using the Mark Houwink equation (eqn (6)) with $k$ and $\alpha$ values, 0.00052 dL g$^{-1}$ and 0.695, respectively.[49,50]

Relative viscosity

$$n_{rel} = \frac{t}{t_0} \quad (1)$$

Specific viscosity

$$n_{sp} = \frac{t - t_0}{t_0} = n_{rel} - 1 \quad (2)$$

Reduced viscosity

$$n_{sp} = \frac{t - t_0}{t_0 * c} = \frac{n_{sp}}{c} \quad (3)$$

Inherent viscosity

$$n_{sp} = \ln\frac{\frac{t}{t_0}}{c} = \left(\frac{\ln(n_{rel})}{c}\right) \quad (4)$$

Intrinsic viscosity

$$[n] = \lim_{c\to 0}\left(\frac{n_{sp}}{c}\right) = \lim_{c\to 0}\left(\frac{\ln(n_{rel})}{c}\right) \quad (5)$$

Mark–Houwink

$$\eta = kM_v^{\alpha} \quad (6)$$

### Differential scanning calorimetry (DSC)

The Differential Scanning Calorimetry (DSC) Q200 curves of the depolymerization product (3–7 mg) were measured in a Hermetic aluminum pan. In the DSC run, the sample was equilibrated at 50 °C before being heated to 280 °C for Polyethylene Terephthalate (PET) with a ramp of 10 °C min$^{-1}$. PET was heated to 280 °C as literature has shown PET melts at 260 °C.[51,52] This ramp rate was chosen to inhibit recrystallization during scanning.[53] Enthalpies of melting of the PET samples were determined by measuring the heat flow associated with the melting of PET from the first cycle.[54] The percent crystallinity of each sample was calculated by dividing the enthalpy of the melting of a PET sample by the enthalpy of 100% crystalline PET (140 J g$^{-1}$).[55]

### Small and wide-angle X-ray scattering (SAXS/WAXS)

The small and wide-angle X-ray scattering of the samples were obtained using a Xenocs Xeuss 3.0 X-ray scattering instrument. These data were collected using a copper source and a PILATUS3 detector. The sample to detector distance of 0.9 m provided small angle data, while a sample to detector distance of 0.045 m provided wide angle data. The obtained scattering data is corrected for sample thickness and sample holder scattering and then reduced to an absolute scale by normalizing the data to the transmitted beam intensity.

### Film casting & tensile testing

Films for mechanical testing were made from virgin PET, PET–PEO MBCP, and a compatibilized blend of 80 : 20 PET : PEO with 1 wt% PET–PEO MBCP. A sample (0.5 g) was dissolved in ~3 mL of HFIP. Excess HFIP was removed by rotary evaporation, yielding a viscous solution. The solution was poured onto a level, clean glass sheet. A film of the concentrated sample solution was formed by using the BYK Film Applicator (bar-shaped Article No. 5302 Double Bar) to create films from a bar gap clearance of 10 mm. This film was covered with aluminum foil to prevent particulates from sticking to its surface as it dried. After fully air-drying, the sheet was removed from the glass and dried in a vacuum oven at 70 °C for 8 h. The sheets were then cut into dog bones using a Carver Model C Laboratory Press and a sharp dog bone mold. The mechanical properties of the materials were tested using an Instron 5965.

### Water swelling

Dog bones made from virgin PET, PET–PEO MBCP, and a compatibilized blend of 80 : 20 PET : PEO with 1 wt% PET–PEO MBCP were used for water swelling experiments. A 10 mg sample was added to 10 mL of water in a vial and placed on an orbital shaker to agitate for varying durations (days). At certain times, the dog-bone sample was removed from the water, dabbed onto filter paper, and weighed. Once the sample is weighed, the dog bone sample is placed back in the water and on the orbital shaker for further measurements at a later time. The percentage of water in the sample was calculated using eqn (7) by comparing the initial weight ($W_i$) to the sample weight at a specific time ($W_t$).

$$\%\text{Swell}_{water} = \frac{W_t - W_i}{W_i} \times 100 \quad (7)$$

### Permeation experiments

**Membrane preparation.** Polymers were cast into membranes *via* solution casting from 3 wt% polymer solutions in HFIP. For example, polymer (0.1 g) and HFIP (2 mL) were combined in a vial containing a magnetic stir bar and stirred until fully dissolved. The resulting polymer solution was filtered through a 0.45 μm PTFE syringe filter into a 6.5 cm diameter glass dish with a cellophane bottom. The dishes were covered with aluminum foil to enable slow solvent evaporation over 48–72 h. The free-standing membranes were then removed from their casting dishes and used as prepared for all subsequent testing.

**Permeation analysis.** Polymer membrane samples were placed over a 1.2 cm-diameter hole in a brass sample holder disk. The edges of each sample were then glued to the brass

disk using an epoxy resin and cured for 2 h. Excess polymer extending beyond the epoxy ring was trimmed, and the sample was mounted in the permeation testing device. Pure gas flux was measured with a constant-volume, variable-pressure permeation system, wherein flux data were used to calculate permeability coefficients according to eqn (8).

$$\text{Permeability} = \frac{V_d l}{P_u A R T}\left[\left(\frac{dP_d}{dt}\right)_{ss} - \left(\frac{dP_d}{dt}\right)_{leak}\right] \quad (8)$$

The downstream volumes ($V_d$) were measured using sequential Burnett expansions with He gas, as reported in the literature.[56] Membrane thicknesses ($l$) were measured directly using a Mitutoyo 293-832-30 digital micrometer and ranged from 80 to 150 μm. Upstream pressure ($P_u$) was recorded as a time-weighted average during steady-state flux measurements. The effective membrane surface area ($A$) was determined using the open-source image analysis software ImageJ, based on images captured with an Epson Perfection V19 flatbed scanner. The gas constant is defined as $R$ = 0.278 [cm Hg cm$^3$] [cm$^3$(STP) K], and temperature ($T$) was measured with an analog alcohol thermometer mounted directly outside the permeation cell.[56]

# Results & discussion

### Model HDI-mediated polymerization or end-capping?

To determine whether excess diisocyanate ultimately produces permanently end-capped oligomers or whether further coupling occurs at longer times, we first examined the HDI-mediated polymerization of BHET and dihydroxy-terminated PEO as chemically well-defined model systems (Fig. 1a). Establishing this behavior in simple, controlled systems is essential for later achieving predictable control over HDI-mediated PET–PEO copolymerization. Polymerizations were conducted at equimolar (OH : NCO = 1 : 1) and excess isocyanate (OH : NCO = 1 : 2) ratios to contrast conditions typically associated with chain extension *versus* end-capping. Polymerizations of BHET–PEO multiblock copolymers (MBCPs) were also examined as a model system. Fig. S2 and S3 show the FTIR spectra of repolymerized PEO (rPEO) and BHET–PEO polymers prepared *via* diisocyanate coupling, highlighting the disappearance of the isocyanate band as the urethane group forms. Fig. S4 and S5 show the $^1$H NMR spectra of BHET, PEO, and BHET–PEO copolymers, and the DOSY NMR spectrum of BHET–PEO, to demonstrate the con-

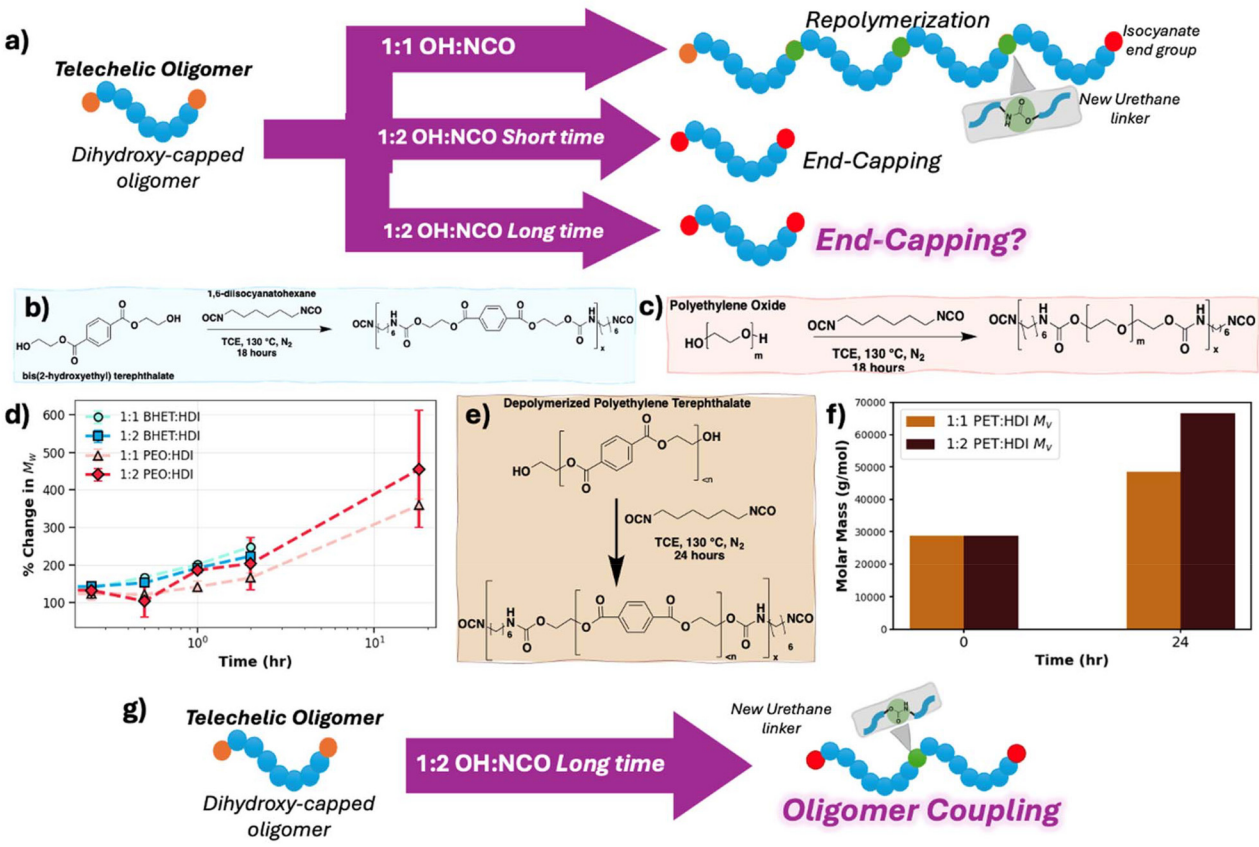


**Fig. 1** (a) Proposed mechanism: OH : NCO = 1 : 1 leads to telechelic oligomer chain extension, whereas OH : NCO = 1 : 2 initially produces end-capped telechelic oligomers; we test whether these species remain end-capped or later couple. (b) BHET polymerization scheme with HDI. (c) PEO polymerization scheme with HDI. (d) Percent change in %$M_w$ for BHET and PEO under OH : NCO = 1 : 1 (light blue/red) and 1 : 2 (blue/red). (e) PET oligomer polymerization scheme with HDI. (f) Viscosity-average molar mass ($M_v$) of PET oligomers at OH : NCO = 1 : 1 (light brown) and 1 : 2 (brown). (g) Graphical conclusion supporting oligomer–oligomer coupling for telechelic oligomers at OH : NCO = 1 : 2 at longer times.

nectivity of the new MBCP formed. Fig. 1b and c summarizes the HDI-mediated coupling schemes for BHET and PEO, and Fig. 1e shows the analogous scheme for PET oligomer polymerization with HDI. Fig. S6 shows the molar mass evolution of repolymerized BHET (rBHET) (equimolar and excess isocyanate), rPEO (equimolar and excess isocyanate), and BHET–PEO copolymer (equimolar) as a function of reaction time as determined by GPC.

Fig. 1d quantifies the time- and stoichiometry-dependent evolution of molar mass in the BHET and PEO model systems. For both BHET and PEO, polymerizations conducted at a 1 : 1 equimolar OH : NCO ratio, as shown in Fig. S6, exhibited the expected increase in number- and weight-average molar masses ($M_n$ and $M_w$) with reaction time, consistent with step-growth urethane formation. More importantly for our central question, reactions performed with excess isocyanate (OH : NCO = 1 : 2), conditions often assumed to yield solely end-capped, growth-arrested oligomers, also showed substantial increases in $M_w$ over time (Fig. S6). To directly compare the extent of growth, Fig. 1d displays the percent change in $M_w$ over time for BHET with equimolar (1 : 1, light blue) and excess isocyanate (1 : 2, blue), as well as for dihydroxy PEO with equimolar (1 : 1, light red) and excess isocyanate (1 : 2, red) relative to hydroxyl end groups. When normalized to the initial molar mass, both BHET and PEO systems exhibit continuous increases in $\%M_w$ with reaction time, reaching several-hundred-percent increases at extended times. Rather than plateauing at a fixed oligomer size, even the nominally "end-capping" 1 : 2 conditions support ongoing coupling events. These results demonstrate that excess HDI does not simply terminate growth but can sustain continued chain extension and/or oligomer–oligomer coupling over long times, challenging the assumption that 1 : 2 conditions produce permanently end-capped, growth-arrested species.

These results indicate that HDI-mediated coupling remains active at this high temperature (130 °C), likely due to secondary reactions involving residual hydroxyl groups, urethane exchange,[57–59] or isocyanate-terminated chain–chain coupling.[60] At this temperature, equilibrium strongly favors monomeric HDI over uretdione formation (dimerization of two –NCO groups), indicating that urethane exchange and hydroxyl-mediated reactions are more likely contributors to the observed coupling behavior than persistent isocyanate–isocyanate coupling.[61] We emphasize that our assignment of ongoing oligomer–oligomer coupling under 1 : 2 OH : NCO conditions is based on time-resolved molecular-weight evolution in BHET, PEO, and dPET oligomeric models (Fig. 1e and f). While these experiments strongly support the presence of secondary coupling pathways such as urethane exchange and reactions of residual hydroxyl groups with isocyanate-terminated species, a definitive discrimination among individual side reactions would require targeted small-molecule end-group models, which we identify as an important avenue for future mechanistic work.

Importantly, the persistence of molar mass growth under excess isocyanate conditions demonstrates that extended reaction times can promote unintended oligomer–oligomer coupling rather than simple end-functionalization. Even with equimolar ratio of OH : NCO, prolonged reaction times are needed to reach a polymer of significant molar mass. We ascribe this behavior to the aliphatic chain in HDI acting as an electron-donating group and lowering the reactivity of the isocyanate, and the slower reaction rate of the second isocyanate within the diisocyanate with a hydroxyl group relative to rate of the first isocyanate reacting with a hydroxyl group.[62–65]

Building on these model studies, BHET and PEO were subsequently polymerized together using HDI at a 1 : 1 OH : NCO ratio to generate a BHET–PEO multiblock copolymer. GPC analysis (Fig. S6c) reveals a monotonic increase in $M_n$ and $M_w$ with reaction time, accompanied by a stabilization of dispersity ($Đ$) after the initial stages of polymerization, consistent with step-growth block copolymer formation between aromatic BHET-derived segments and flexible PEO chains. Taken together, the BHET and PEO model systems demonstrate that HDI-mediated coupling reactions remain kinetically active over extended timescales, even under conditions typically associated with end-capping. These findings directly inform the subsequent synthesis of PET–PEO multiblock copolymers from recycled PET oligomers, where controlling end-capping time is critical to suppress PET–PET coupling prior to PEO incorporation.

Fig. 1f extends this mechanistic picture from the well-defined diol models to a realistic depolymerized PET (dPET) feedstock, where control over end-capping is critical for subsequent block copolymer formation. Unlike the model diols, dPET obtained *via* glycolysis is chemically heterogeneous, with a distribution of chain lengths and multiple hydroxyl functionalities per chain.[30] PET oligomers generated by glycolysis were therefore first characterized with respect to molar mass and average hydroxyl content per chain. As summarized in Table S1, dPET trial 1 exhibits an $M_v$ of ~28 kg mol$^{-1}$, $Đ$ of 1.73, and an average of 1.71 hydroxyl end groups per chain. Repolymerization reactions were then carried out with dPET and HDI at 1 : 1 and 1 : 2 OH : NCO ratios to form repolymerized PET (rPET). Fig. S7 shows the $^1$H NMR spectra of dPET trial 1 and rPET at both stoichiometries, confirming the disappearance of hydroxyl end-group signals in rPET relative to dPET. The rPET samples shown in Fig. S7 were prepared as model repolymerization systems to probe molecular-weight growth under 1 : 1 and 1 : 2 OH : NCO conditions. After 24 h, these reactions were terminated by the addition of isopropanol (IPA), which reacts with residual isocyanate groups to form urethane-linked isopropoxy end groups. The resulting rPET materials were not used as precursors for multiblock copolymerization; they serve solely to demonstrate the ability of HDI to re-polymerize depolymerized PET chains with excess isocyanate.

Within this context, Fig. 1f quantifies the impact of stoichiometry and reaction time on PET chain growth: the viscosity-average molar mass ($M_v$) of dPET trial 1 increases between 0 and 24 h for both 1 : 1 and 1 : 2 PET : HDI formulations, with higher $M_v$ values observed under the more isocyanate-rich 1 : 2 conditions, consistent with more extensive chain

extension and/or mild branching. Substantial molar mass growth is observed even under conditions nominally intended to favor end-capping, indicating that PET–PET coupling readily occurs during extended HDI exposure and mirroring the behavior observed in the BHET and PEO model systems (Fig. 1d and Fig. S6).

Taken together with the mechanistic schematics in Fig. 1a and 1g, Fig. 1d and 1f reveal a unified picture: in both simple diol models and depolymerized PET, excess HDI does not lock oligomers into permanently end-capped structures but instead allows continued molar mass growth over time. This insight, that 1 : 2 OH : NCO conditions do not guarantee static end-capped species but can lead to ongoing oligomer-oligomer coupling at longer times (Fig. 1g), is critical for rationally controlling HDI-mediated PET–PEO multiblock formation. These results motivate the use of short HDI end-capping times prior to PEO addition in order to bias multiblock formation *via* PET–PEO linkages rather than uncontrolled PET–PET coupling, as explored in the following section. On the basis of these observations, a short end-capping protocol (10 min) was selected prior to PEO addition for the synthesis of PET–PEO multiblock copolymers, while extended end-capping (24 h) was intentionally examined as a contrasting condition to probe the consequences of uncontrolled chain–chain coupling.

### PET-PEO copolymerization

Virgin PET was depolymerized to ensure that dihydroxy-capped oligomers with an $M_n$ similar to the 4 kg mol$^{-1}$ PEO were produced, so that, ideally, this 50 : 50 multiblock copolymer will exhibit properties of both parent polymers.[66–69] All depolymerized PET samples used here were derived from bottle-grade PET, and independent depolymerization trials (Tables S1 and S2) produced dihydroxy-terminated oligomers with similar molar mass and end-group densities. Under identical PET–HDI–PEO conditions, these different dPET batches yielded PET–PEO multiblock copolymers with comparable molar mass and PET/PEO ratios for a given end-capping time, indicating that the synthetic strategy is reproducible across batches of bottle-derived PET, although extension to other PET sources remains a subject for future work.

Fig. S8 shows the GPC traces of virgin PET and the dPET trials 2 and 3; the depolymerized samples exhibit later retention times and therefore lower molar masses than virgin PET. Fig. S9 shows the $^1$H NMR spectra of virgin PET and the dPET trials 2 and 3; the depolymerized samples exhibit greater integration for the methylene peaks in the alpha position to the hydroxyl end group, indicating an increase in the average number of hydroxyl end groups per chain compared to virgin PET. Table S2, which shows $M_n$, $m_w$, $Đ$, and average number of –OH end groups, quantifies the chain length by showing that dPET trial 2 ($M_n$ = 5.5 kg mol$^{-1}$, $Đ$ = 1.88, 2.0 –OH end groups) and trial 3 ($M_n$ = 5.7 kg mol$^{-1}$, $Đ$ = 1.53, 1.97 –OH end groups) decreases in molar mass and increases in average number of hydroxyl end groups compared to virgin PET ($M_n$ = 15.98 kg mol$^{-1}$, $Đ$ = 1.97, 1.13 –OH end groups). Table S2 also demonstrates that dihydroxy-capped oligomers with an $M_n$ similar to the 4 kg mol$^{-1}$ PEO have been isolated. For the short-term end-capping (10 min) reaction, dPET trial 2 was used, and for the long-term end-capping (24 h) reaction, dPET trial 3 was used. Since TBD is used as a TBD : MSA organo-salt and the dPET oligomers undergo triple HFIP/MeOH precipitation prior to coupling, it is unlikely that any residual basic catalyst is present to enable further transesterification during PET–PEO synthesis.

Fig. 2 illustrates the copolymerization of PET and PEO utilizing short-end capping. Fig. 2(a) illustrates the reaction scheme for the short end-capping (10 min) of dPET followed by the subsequent addition of PEO. While temperature is expected to influence reaction kinetics and urethane exchange, PET solubility in TCE constrained our experiments to a narrow

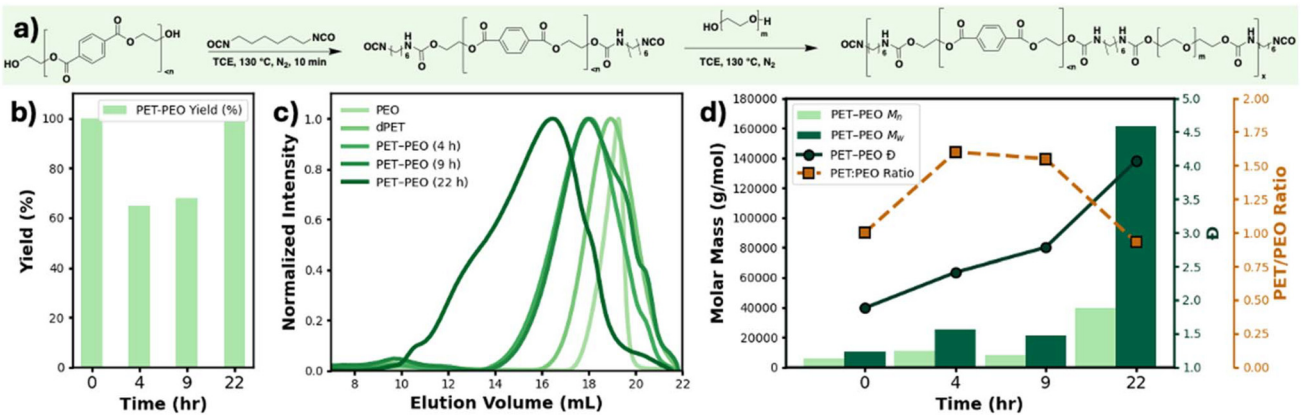


Fig. 2 (a) Reaction scheme illustrating short HDI end-capping of PET oligomers (10 min end-capping time), followed by subsequent addition of PEO. (b) Isolated yield of PET-PEO multiblock copolymer as a function of reaction time (0, 4, 9, and 22 h) following short end-capping. (c) GPC traces of PET-PEO samples collected at 0, 4, 9, and 22 h, showing progressive increases in molar mass with reaction time. (d) Evolution of molar mass ($M_n$, light green bars; $M_w$, green bars), dispersity ($Đ$, dark green line), and PET/PEO ratio (dashed brown line) during PET–PEO multiblock formation. The PET/PEO ratio is defined as the $^1$H NMR-derived PET proton fraction divided by the theoretical value expected for ideal 1 : 1 PET–PEO oligomer incorporation.

temperature window around 130 °C. Systematic variation of temperature in alternative solvent systems that maintain PET solubility represents an important avenue for future optimization of multiblock architecture and dynamics. Fig. 2(b) shows the isolated yield of the PET–PEO multiblock product as a function of reaction time. Fig. 2(b) shows that the final 22 h sample is obtained in high yield, indicating that most of the reactive material is incorporated into the recovered copolymer. Intermediate samples taken at 4 and 9 h exhibit somewhat lower apparent isolated yields, suggesting that a fraction of shorter, incompletely coupled species is more easily lost during the IPA/hexane precipitation and washing steps.

Fig. 2(c) shows the GPC curves of each sample. Fig. 2(d) shows the evolution of molar mass ($M_n$-light green bar, $M_w$-green bar), $Đ$ (dark green line), and block copolymer composition (PET/PEO ratio determined by $^1$H NMR spectroscopy, dashed brown line) over 0, 4, 9, and 22 h during PET-PEO multiblock formation using the dPET that is end-capped with a 10 min (short) HDI end-capping reaction. Fig. S10 shows that, after PEO addition, NMR reveals no residual hydroxyl end groups and an increase in urethane-group intensity with reaction time, indicating rapid consumption of residual isocyanate end groups. Fig. S11 shows DOSY NMR of each sample to demonstrate the connectivity of the oligomers. Equations S1-S4 demonstrate how $^1$H NMR spectroscopy was used to quantify the PET/PEO ratio by integrating aliphatic proton resonances unique to each oligomer. Eqn (S1) utilizes $M_n$ to calculate the degree of polymerization ($n$) by dividing $M_n$ by the monomer repeat-unit molar mass ($M_o$). Eqn (S2) obtains the total aliphatic protons in the polymer ($H_{polymer}$) from $n$ and the number of aliphatic protons per repeat unit ($H_{monomer}$). For PET–PEO multiblock copolymers, eqn (S3) finds the PET proton fraction ($f_{PET}$) is defined as PET aliphatic protons divided by the total aliphatic protons from PET and PEO. This PET fraction is then normalized to an ideal 1 : 1 PET : PEO composition in eqn (S4) using the ratio $f_{PET\text{-}observed}/f_{PET\text{-}expected(1:1)}$. In a specific 1 : 1 dPET trial 2/PEO system, the expected PET proton fraction is 0.24, and experimental values are compared to this reference. Table S3 shows the theoretical PET proton fraction expected for ideal 1 : 1 PET–PEO oligomer incorporation for both dPET trials 2 and 3, the observed PET fraction for the short end-capped PET–PEO with reaction time, and the observed PET proton fraction for the long end-capped PET–PEO samples. Table S3 also reports the PET/PEO ratio, defined as the ratio of the observed PET proton fraction to the theoretical value expected for ideal 1 : 1 incorporation, and illustrates the molar ratio of PET repeat units to PEO repeat units in the multiblock copolymer, determined from $^1$H NMR peak integrals. Ideal stoichiometry would yield a PET/PEO ratio of 1.0. However, if the PET/PEO ratio is >1.0, more aliphatic PET protons are observed than expected for a 1 : 1 incorporation of PET and PEO, indicating a lack of PEO incorporation/blocks. Likewise, if the PET/PEO ratio is <1.0, fewer aliphatic PET protons are observed than expected, indicating over incorporation of PEO blocks and deviation from the ideal 1 : 1 incorporation.

We emphasize that the PET–PEO multiblock copolymers are prepared in a single-pot PET–HDI–PEO process: the PET oligomers are first end-capped with HDI, PEO is then added to the same reaction mixture, and finally all residual –NCO groups are consumed by an isopropanol quench. Together with DOSY NMR (Fig. S11 and S13) and $^1$H NMR composition analysis (Table S3), this protocol minimizes the formation of isolated PEO–HDI species and verifies that PET and PEO segments are covalently incorporated into the same diffusing macromolecules.

As the reaction in Fig. 2(d) proceeds for 4 h, $M_w$ increases substantially, whereas $M_n$ increases more modestly, consistent with step-growth multiblock formation accompanied by an increase in $Đ$. The 0 h period exhibits a PET proton fraction consistent with a 1 : 1 molar mixture of PET and PEO oligomers, indicating the presence of uncoupled homopolymers, since no polymers are covalently bonded at this stage. During the reaction workup (4–22 h), the $^1$H NMR spectrum shows only multiblock copolymer (MBCP) resonances, indicating successful coupling.

Notably, the PET/PEO ratio determined by $^1$H NMR reaches a maximum at early reaction times (4–9 h), indicating PET enrichment relative to ideal PET–PEO incorporation. In those same samples, limited molecular-weight growth by GPC is exhibited; this behavior is consistent with incomplete heterocoupling, in which a fraction of PET oligomers remains uncovalently bonded to PEO. At longer reaction times (22 h), $M_w$ increases sharply to >160 kg mol$^{-1}$, accompanied by a concurrent rise in $Đ$, while the PET/PEO ratio decreases toward unity. This trend reflects increasing PET–PEO incorporation toward the theoretical 1 : 1 composition, consistent with progressive step-growth coupling. The alternating nature of the PET and PEO blocks in this 22 h multiblock copolymer most closely resembles segmented block copolymers of existing long-soft-segment polyethers and long-hard-segment (sometimes crystalline) polyurethanes.[70–72] Consistent with this picture, the short-end-capped 4 and 9 h samples, which display PET-enriched PET/PEO ratios (~1.55–1.60), also exhibit lower isolated yields than the fully reacted 22 h sample. We infer that in these short reaction times, the uncoupled PEO oligomers are preferentially lost during IPA/hexane work-up, whereas more completely coupled PET–PEO chains are fully recovered.

Although $^1$H NMR spectra do not directly resolve block number or sequence, the convergence of PET/PEO ratio toward unity at longer reaction times, together with substantial molar mass growth observed by GPC, supports formation of PET–PEO multiblock copolymers with near-stoichiometric segment incorporation. Together, these results demonstrate that short HDI end-capping, followed by controlled polymerization times, enables PET–PEO multiblock formation while minimizing uncontrolled PET–PET coupling, consistent with trends observed in the BHET/PEO model system.

Table 1 demonstrates the influence of HDI end-capping time on PET–PEO multiblock formation by comparing polymers prepared using short (10 min or 0.167 h) and extended

**Table 1** Comparison of PET–PEO multiblock copolymers prepared using short (10 min) and extended (24 h) HDI end-capping prior to PEO addition, showing number-average molar mass ($M_n$), weight-average molar mass ($M_w$), dispersity ($Đ$), observed PET proton fraction (expressed as PET/PEO ratio from $^1$H NMR), and isolated yield

| End-capping Time (h) | $M_n$ (kg mol$^{-1}$) | $M_w$ (kg mol$^{-1}$) | $Đ$ | PET/PEO ratio | Yield |
|---|---|---|---|---|---|
| 0.167 | 40 | 161 | 4.1 | 0.93 | 98.9% |
| 24.0 | 29 | 108 | 3.8 | 1.67 | 100.6% |

(24 h) HDI end-capping of PET prior to PEO addition. Fig. S12 shows the GPC traces of both PET-PEO multiblock copolymers. Despite comparable molar masses, the two materials exhibit distinct PET/PEO ratios and $Đ$, reflecting differences in segment incorporation arising from fundamentally different reaction pathways. The PET–PEO formed from the 10 min end-capped dPET exhibits a PET/PEO ratio of 0.93, consistent with near-stoichiometric PET–PEO incorporation despite rapid consumption of PET hydroxyl end groups and minimal PET–PET self-coupling prior to PEO addition. In contrast, extending the end-capping time of the dPET to 24 h yields a substantially elevated PET/PEO ratio (1.67), indicating PET enrichment relative to ideal PET–PEO coupling. This behavior is consistent with significant PET–PET chain extension occurring during prolonged exposure of dihydroxy-terminated PET to HDI prior to PEO addition, likely *via* secondary isocyanate coupling.

This interpretation is further supported by the observed increase in molar mass during extended PET–HDI end-capping reactions, as well as by analogous trends in the BHET and PEO model systems. Additionally, Fig. S13 shows DOSY NMR analysis of the 24 h end-capped sample, which shows a single diffusing species for PET and PEO resonances, confirming covalent incorporation of both segments while remaining insensitive to block sequence or relative block abundance. Although the 24 h end-capped material exhibits a slightly lower $Đ$ than the 10 min sample, its elevated PET/PEO ratio indicates a reduced effective PEO incorporation into the multiblock and diminished control over multiblock connectivity.

Collectively, these results demonstrate that HDI end-capping time is a critical synthetic parameter governing relative PET–PEO segment incorporation and multiblock composition and connectivity. Short times to end-cap dPET with HDI favor the formation of targeted PET–PEO multiblock with PET–PEO connectivity, while minimizing uncontrolled PET–PET coupling. In summary, Fig. 3 illustrates our identification of a flexible synthetic strategy to upcycle depolymerized PET into PET–PEO multiblock copolymers by intercepting dihydroxy-terminated telechelic oligomers and using HDI-mediated urethane coupling. Model studies with BHET and PEO establish predictable polymer growth and highlight the sensitivity of chain extension to isocyanate stoichiometry and reaction time. Translation of this approach to the formation of multi-block copolymers using depolymerized dihydroxy-terminated PET oligomers as feedstocks reveals that HDI end-capping time of the dPET oligomers serves as a key architectural control parameter, governing PET–PET coupling relative to PEO incorporation and directly dictating multiblock composition. By focusing on short end-capping time, PET–PEO copolymers with controlled PET/PEO ratio and high molar masses are obtained, providing a chemically tunable platform to probe structure–property relationships in upcycled materials. Having established synthetic control over PET–PEO multiblock architecture, we next examine how end-capping time and block composition influence the mechanical performance of solvent-cast films.

### Mechanical properties of PET–PEO multiblock copolymers

The mechanical properties of the synthesized PET–PEO multiblock copolymers provides important insight into the molecular structure-macroscopic property relationships that emerge from the variation in molecular architecture and phase behavior introduced by end-capping and copolymer formation. Fig. 4 illustrates images of thin film samples (a), the average tensile stress–strain curves (b) and average tensile strength *vs.* strain at break (c) for virgin PET (black), PET–PEO (24 h end-capped: dark green), PET–PEO (10 min end-capped: light green), rPET (brown), 80 : 20 PET/PEO Homopolymer Blend (light brown), 80 : 20 PET/PEO compatibilized blend (blue). Fig. S14–S17 show the tensile stress–strain curves for each virgin PET, PET–PEO (24 h end-capped), PET–PEO (10 min end-capped) sample, and compatibilized PET/PEO 80 : 20 blend. Fig. S18 illustrates thin film images of failed solvent cast films for a 50/50 blend of PET : PEO homopolymers, a 50/50 blend of PET : PEO homopolymers that were compatibilized with 1 wt% of the short end-capped PET-PEO MBCP and repolymerized PEO (38.3 kg mol$^{-1}$).

In Fig. 4, the properties of the virgin PET ($M_v \approx 54$ kg mol$^{-1}$) demonstrate the expected high tensile strength and low strain at break, reflecting its semicrystalline, rigid backbone. In contrast, the depolymerized PET ($M_v \approx 28$ kg mol$^{-1}$) is repolymerized *via* HDI-mediated coupling, resulting in higher-molecular-weight materials ($M_v \approx 66$ kg mol$^{-1}$) composed of PET blocks connected by short aliphatic urethane linkers. Fig. 4(d) shows the DSC curves for both virgin (black) and repolymerized (brown) PET, indicating a decrease in the melting peak temperature for rPET. Table S4 reports the heats of fusion for virgin and rPET, indicating a reduction in both the heat of fusion and percent crystallinity for the repolymerized PET. Although this process increases molar mass, the incorporation of flexible HDI segments disrupts the regular aromatic ester backbone of PET, decreasing crystallinity and creating more compliant junctions between rigid PET domains. Consequently, repolymerized PET exhibits a modest reduction in tensile strength compared to virgin PET, despite maintaining or slightly improving ductility.[73–78]

Incorporation of PEO dramatically alters the mechanical response of the polymer, with clear distinctions observed between the copolymer synthesized from variations in the end-capping conditions and thus copolymer connectivity. The PET–PEO multiblock prepared from 24 h HDI end-capped dPET (Fig. 4(b and c), dark green) exhibits the highest tensile strength among the virgin or upcycled materials while main-

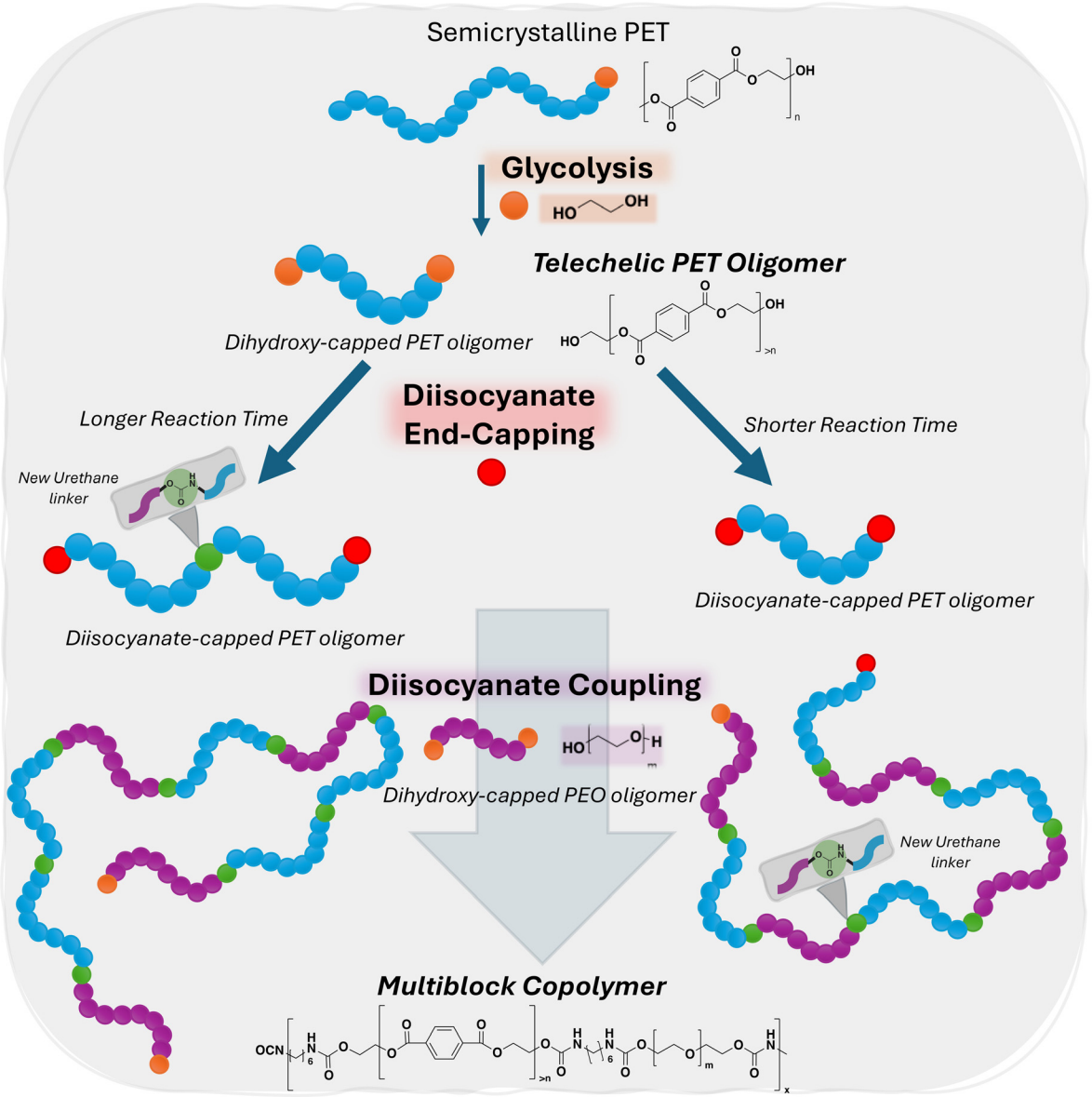


**Fig. 3** Modular synthetic strategy for PET–PEO multiblock copolymers. Depolymerized PET is converted to telechelic oligomers *via* glycolysis, end-capped with HDI, and subsequently coupled with PEO to form multiblocks. HDI end-capping time controls the balance between PET–PET self-coupling and PET–PEO incorporation, enabling tunable multiblock composition and molar mass.

taining substantial extensibility, indicating effective load transfer across hard PET domains and soft PEO segments.[79–81] Fig. 4(d) and Table S4 show that 24 h end-capped PET–PEO (dark green) has a melting peak and heat of fusion for PET ($T_m2$), but not for PEO ($T_m1$), consistent with the idea of hard PET domains and soft PEO segments. This is consistent with the general behavior of crystalline–crystalline multiblock copolymers, in which overall crystallinity can be strongly suppressed when one block is significantly longer than the other due to confinement and dilution effects.[82–86] This behavior is consistent with GPC and $^1$H NMR results, which indicate increased molar mass and a higher PET/PEO ratio (1.67) relative to the 10 min end-capped sample (0.93). As previously shown in Fig. 1(f), control experiments in which PET was repolymerized for 24 h at 1 : 1 and 1 : 2 OH : NCO molar ratios showed molar mass growth in all cases, supporting the conclusion that extended end-capping promotes PET–PET coupling prior to PEO incorporation. As a result, the 24 h end-capped material likely contains longer PET blocks, thereby enhancing mechanical reinforcement.

In contrast, the PET–PEO sample synthesized using 10 min HDI end-capped dPET (Fig. 4(b and c), light green) exhibits significantly higher strain at break but reduced tensile strength, consistent with shorter PET segments and a higher effective PEO content. The increased chain mobility due to more PEO content in the multiblock enhances ductility but

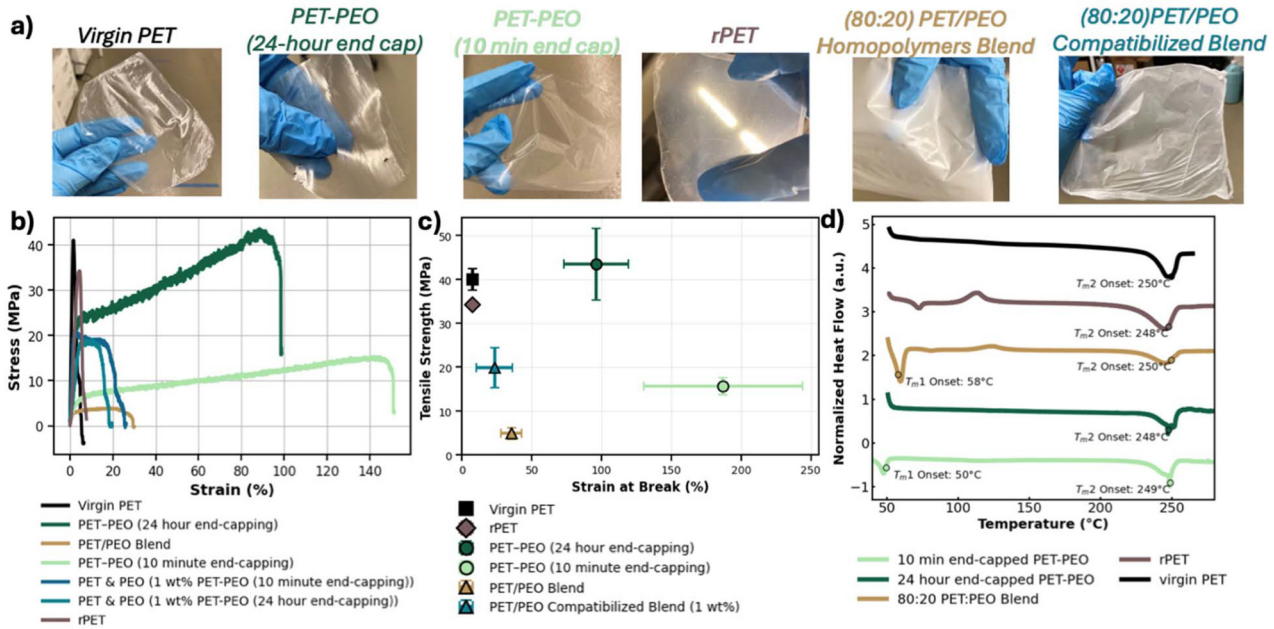


**Fig. 4** (a) Representative sheet images, (b) tensile stress-strain curves, and (c) average tensile strength *versus* strain at break for virgin PET (black), PET–PEO with 24 h HDI end-capping (dark green), PET–PEO with 10 min HDI end-capping (light green), rPET (brown), an 80 : 20 PET/PEO homopolymer blend (light brown), and an 80 : 20 PET/PEO compatibilized blend (blue). (d) DSC traces (exo down) of virgin PET (black), rPET (brown), PET-PEO with 10 min HDI end-capping (light green), PET–PEO with 24 h HDI end-capping (dark green), and the 80 : 20 PET/PEO blend (light brown), where melting peaks associated with PEO ($T_m1$) and PET ($T_m2$) are labeled.

limits stress-bearing capability.[87] The mechanically distinct responses of these two multiblocks directly reflect differences in copolymer sequence length and block connectivity imposed by the end-capping duration.[67,88–90] Fig. 4(d) and Table S4 support this interpretation: the 10 min end-capped PET-PEO sample (light green), which has comparable PET and PEO block lengths (~4–5 kg mol$^{-1}$), exhibits measurable heats of fusion for both PET ($T_m2$) and PEO ($T_m1$), indicating that both blocks can crystallize. In contrast, in the 24 h end-capped sample, the PET block is significantly longer while the PEO block remains short (~4 kg mol$^{-1}$). By controlling the end-capping time, we can tune the suppression of PEO crystallinity: short end-capping minimizes suppression because PET and PEO have similar block lengths. Conversely, the extended end-capping produces a strongly asymmetric sequence distribution with longer, higher-$T_m$ PET blocks and shorter PEO blocks. We interpret the DSC data to indicate that PET crystallizes first, forming a continuous hard phase that spatially confines and effectively dilutes the short, tethered PEO segments. Such block-length asymmetry in linear crystalline-crystalline multiblocks is known to suppress overall crystallinity, as the short blocks lack sufficient length to form stable nuclei and are locally constrained, which will prevent the formation of well-developed PEO lamellae.[82–86] Consistent with this picture, PEO crystallinity appears to be strongly suppressed in the 24 h end-capped sample, and no distinct PEO melting peak is observed in the DSC, while PET still shows a clear melting endotherm.

Blending experiments further highlight the importance of multiblock connectivity for macroscopic properties and provide insight into the ability of the upcycled PET–PEO multiblock copolymers to compatibilize PET–PEO blends. These mechanical property studies show that an uncompatibilized 80 : 20 PET : PEO homopolymer blend, shown in Fig. 4(b and c) (light brown), exhibits poor mechanical integrity and reduced strength, indicative of phase separation and weak stress transfer between phases. Consistent with this interpretation, DSC analysis of the 80 : 20 blend (Fig. 4(d) and Table S4) shows distinct melting and heats of fusion for both PET ($T_m2$) and PEO ($T_m1$), indicating that the two components crystallize largely independently rather than forming a nanoscale homogeneous morphology, in contrast to the PET–PEO multiblock copolymers. Although the addition of 1 wt% PET–PEO compatibilizer to an 80 : 20 PET/PEO blend improves film formation and modestly enhances mechanical performance, the compatibilized blend remains substantially weaker than the corresponding multiblock copolymers. Notably, Fig. S18 shows attempts to prepare a 50 : 50 PET : PEO blend using the same compatibilizer loading resulted in catastrophic film failure, underscoring the limits of interfacial stabilization in PEO-rich samples. Together, these results demonstrate that covalent multiblock architectures are substantially more effective than physical blends at maintaining mechanical integrity while incorporating high fractions of flexible, hydrophilic PEO segments.

To further probe the nanoscale structure and crystallinity of these materials, the small- and wide-angle X-ray scattering (SAXS/WAXS) curves of the same solvent-cast films used for mechanical, DSC, and swelling experiments (Fig. S19). The

WAXS patterns confirm the presence of crystalline PET and, where applicable, PEO reflections, consistent with the melting endotherms and heats of fusion obtained by DSC. SAXS profiles exhibit scattering features characteristic of semicrystalline lamellar morphology but do not show well-resolved higher-order peaks that would indicate the formation of microphase separated domains that may be expected of block copolymers. Thus, while X-ray scattering corroborates the existence and relative amount of crystalline phases, DSC provides the more direct insight into which blocks crystallize in each sample and how crystallinity evolves with end-capping time and block architecture.

### Water uptake and swelling behavior

Water-swelling experiments were first conducted to probe the accessibility and connectivity of PEO-rich domains and to assess the extent of water-induced plasticization in PET–PEO materials. Fig. 5 shows the water swelling (%) of virgin PET (black square), PET–PEO copolymer (24 h end-capped: dark green circle), PET–PEO copolymer (10 min end-capped: light green circle), rPET (brown diamond), an 80 : 20 PET/PEO Homopolymer Blend (light brown diamond), an 80 : 20 PET/PEO compatibilized blend (24 h end-capped: light blue triangle), and an 80 : 20 PET/PEO compatibilized blend (10 min end-capped: dark blue triangle) as a function of time exposure to water. Virgin PET exhibits minimal water uptake over the entire experimental timescale, remaining below ~10% swelling even after extended exposure. This behavior is consistent with the hydrophobic, rigid nature of the PET backbone and its limited free volume.

In contrast, Fig. 5 shows that both PET-PEO MBCPs display rapid and substantial water uptake (40–80%), with swelling increasing sharply within the first day and continuing to rise over longer timescales. The magnitude of swelling suggests that PEO-rich segments are readily accessible to water and form continuous or semi-continuous domains that can undergo significant hydration. Notably, the PET–PEO multiblock copolymer synthesized from the dPET that is end-capped for 10 min contains a PET/PEO ratio of 0.93, as determined by $^{1}$H NMR, indicating a high effective PEO content that dominates sorption behavior. Even with a lower PEO incorporation (PET/PEO ratio of 1.67) in the 24 h end-capped multiblock, PEO still dominates sorption behavior. The persistence of swelling over time further suggests that water penetration is not limited to the surface but extends throughout the bulk material.

Compatibilized PET/PEO blends shown in Fig. 5 exhibit intermediate swelling behavior between that of the multiblocks and the PET homopolymer. While water uptake is higher than that of virgin PET, it remains substantially lower than that observed for PET–PEO MBCPs, consistent with partial phase separation and restricted connectivity of PEO domains.[91–93] These results indicate that the morphology formed in these compatibilized blends limits excessive PEO swelling, potentially by constraining domain size and interfacial mobility. At higher overall PEO loadings, however, mechanical integrity is lost, as evidenced by the disintegration of 50 : 50 PET : PEO films even in the presence of identical copolymer content, as shown in Fig. S20. This observation underscores the sensitivity of bulk properties to PEO content, domain connectivity, and morphology.

### Gas permeability

The pronounced differences in water uptake among these materials, shown in Fig. 5, provide important insight into molecular transport through these films and motivate the examination of their gas transport behavior. To assess how polymer architecture influences gas transport, gas permeation

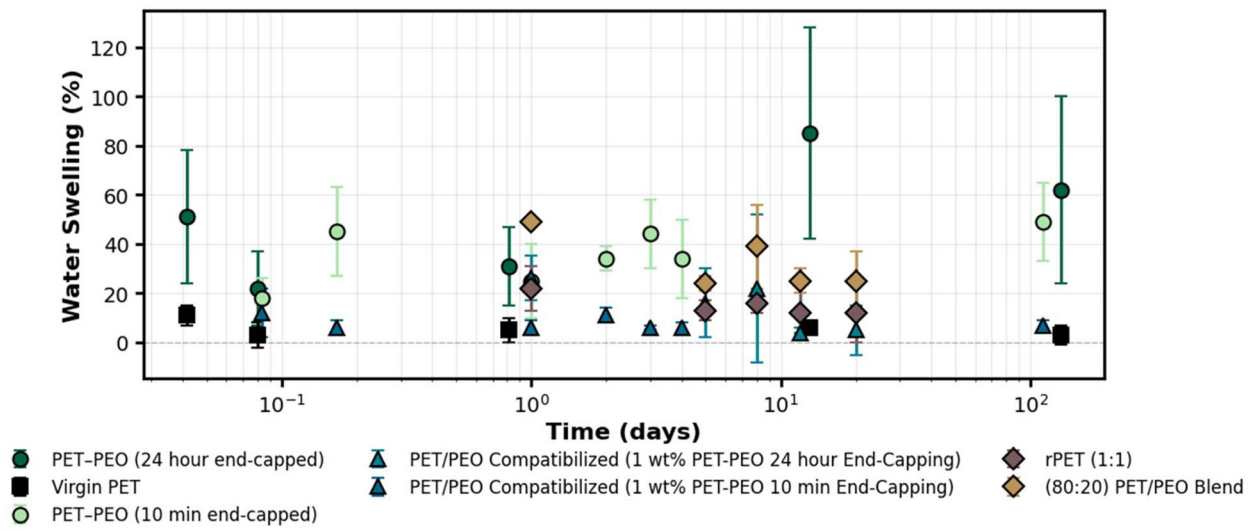


**Fig. 5** Water swelling (%) as a function of log(water exposure time) for virgin PET (black squares), rPET (brown diamonds), PET–PEO multiblocks prepared *via* 24 h (dark green circles) and 10 min (light green circles) end-capping, an 80 : 20 PET/PEO homopolymer blend (light brown diamonds), and 80 : 20 PET/PEO blends compatibilized with 1 wt% PET–PEO (24 h: light blue triangles; 10 min: dark blue triangles).

measurements were performed on free-standing films of compatibilized PET/PEO blends and PET–PEO multiblock copolymers. We hypothesized that materials exhibiting higher water uptake may also exhibit increased gas permeability, particularly for larger, more condensable gases such as $CO_2$ and $CH_4$. $CO_2$ permeability is emphasized as the design-relevant metric because PEO is widely regarded as a $CO_2$-selective block,[94,95] enabling direct comparison between PET-derived multiblock membranes synthesized from recycled consumer waste and established virgin poly(butylene terephthalate) (PBT)–PEO systems used in commercial gas separation membranes. Notably, the PBT–PEO (PolyActive) reference materials employ a block composition of approximately 45 wt% PEO and 55 wt% PBT,[96,97] which closely mirrors the PET-to-PEO ratio of the PET–PEO multiblock copolymers studied here (PET/PEO ratio of 0.93). However, the pure-gas permeation of He, $H_2$, $N_2$, $O_2$, and $CH_4$ is also included to contextualize transport behavior and relative selectivity, as is discussed in the SI.

Gas transport in these dense polymer membranes is governed by the solution-diffusion mechanism, in which permeability reflects the product of gas diffusivity and solubility.[98] In semicrystalline PET-based systems, transport occurs primarily through the amorphous regions, while crystalline domains act as impermeable barriers that restrict segmental motion and reduce available free volume.[99] Consequently, changes in crystallinity, chain packing, and local segmental mobility are expected to strongly influence gas transport behavior.

Based on these considerations, virgin PET is expected to exhibit low permeability with relatively strong molecular discrimination, consistent with its dense, glassy semicrystalline microstructure. Introducing PEO through physical blending is anticipated to increase permeability, but at the expense of transport uniformity due to phase separation within the blend.[100–102] In contrast, PET–PEO multiblock copolymers were expected to exhibit gas transport properties more akin to those observed for other PEO-containing materials[94,95] as the covalent linkage promotes more uniform molecular-level distribution of PEO within the amorphous regions of the semicrystalline PET phase, disrupting local chain packing and increasing segmental mobility without generating the larger-scale transport heterogeneities associated with physical blending.

As an example, Fig. 6 presents the Robeson plot for the $CO_2/CH_4$ gas pair and compares the short end-capped PET–PEO multiblock copolymer (green diamond) to an 80 : 20 PET/PEO blend compatibilized with 1 wt% PET–PEO (orange square), as well as the commercially available gas separation membrane material, PolyActive[80,96,103–105] (blue circle). To further emphasize the comparison between recycled PET-based membranes and virgin commercial materials, Table 2 summarizes the measured permeability values for PET–PEO multiblock copolymers alongside representative PolyActive systems. Table S5 reports the permeability of all samples for various gases, while Fig. S20 presents all available Robinson plots of the tested samples.

Fig. 6 shows that the compatibilized PET/PEO blend exhibits higher $CO_2$ permeability than virgin PET (Table S5), which

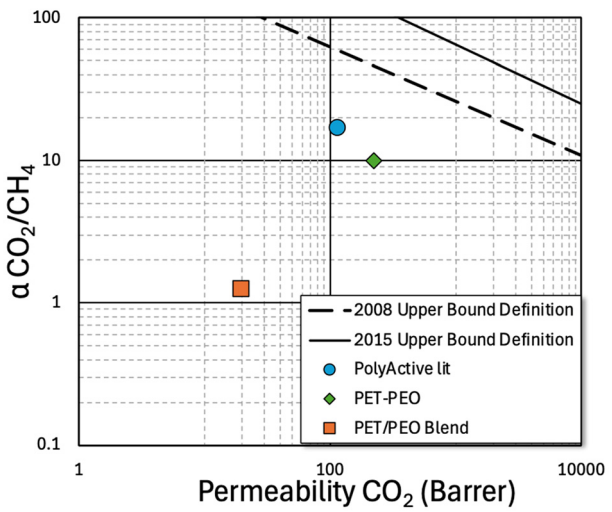


**Fig. 6** Robeson plot showing $CO_2/CH_4$ selectivity *versus* $CO_2$ permeability. Literature data for PolyActive ($4000PEO_{55}PBT_{45}$ [97] and PEO–PBT/GO-0 [96]) and PET of varying densities are shown alongside experimentally measured short-end-capped PET–PEO multiblock copolymer (MBCP) and an 80 : 20 compatibilized PET : PEO homopolymer blend (1 wt% compatibilizer) permeated with the corresponding gases. The 2008 and 2015 Robeson upper bounds are included as references.

**Table 2** Literature values for PolyActive[96,97] experimental values for short-end-capped PET–PEO MBCP permeated with He, $H_2$, $N_2$, $CH_4$, $CO_2$, and $O_2$

| | Permeability (Barrer) | | | | | |
|---|---|---|---|---|---|---|
| Sample | He | $H_2$ | $N_2$ | $CH_4$ | $CO_2$ | $O_2$ |
| PolyActive ($4000PEO_{55}PBT_{45}$)[97] | — | 10.55 | 2.61 | 6.76 | 112 | — |
| PolyActive (PEO-PBT/GO-0)[96] | — | 14.3 | 2.88 | 8.4 | 150 | — |
| PET–PEO (10 min end-capped) | 139 | 244 | 52 | 23 | 224 | 197 |

is consistent with the incorporation of a PEO-containing phase.[94,95] However, this increase in permeability is accompanied by a dramatically lower $CO_2/CH_4$ selectivity than is observed for the PET–PEO multiblock copolymer and PolyActive. This behavior is consistent with the DSC results (Table S4), which show distinct melting endotherms for both PET and PEO in the blend, indicating that the two polymers retain sufficient mobility to crystallize largely independently. Such independent crystallization indicates heterogeneous phase organization and limited molecular-level integration, likely generating interfacial transport pathways that increase permeability but compromise molecular discrimination.[100–102]

In contrast, PET–PEO multiblock copolymers exhibit $CO_2$ permeability comparable to PolyActive, while displaying similar, but not enhanced, $CO_2/CH_4$ selectivity. The thermal and structural characterization provides important insight into the origin of this behavior. DSC reveals strongly suppressed or absent PEO crystallization in several multiblock samples despite significant PEO incorporation, indicating confinement of PEO segments within PET-rich semicrystalline environ-

ments. At the same time, SAXS profiles (Fig. S19) show broad scattering maxima characteristic of semicrystalline lamellar morphology but no higher-order reflections indicative of well-ordered microphase separation. Together, these observations suggest that transport enhancement does not arise from classical microphase-separated diffusion channels, but rather from local disruption of PET chain packing and altered segmental mobility within mixed amorphous regions. This architecture increases gas permeability by increasing local fractional free volume and enhancing $CO_2$ sorption through ether-rich PEO segments, while preserving sufficient structural constraint from PET crystallites to retain moderate molecular discrimination.[106]

The PET–PEO multiblock shows slightly lower $CO_2/CH_4$ selectivity than PolyActive (PBT–PEO), despite comparable permeability. This difference likely reflects intrinsic differences between PET- and PBT-based hard segments, as well as differences in segmental organization. Specifically, PBT has been shown to exhibit intermolecular C═O···H–C hydrogen bonding and reduced chain flexibility relative to PET, owing to its greater number of methylene units, whereas PET weaker and less extensive hydrogen-bonding interactions.[107] FTIR analysis of the present system (Fig. S21) indicates evidence of hydrogen bonding in the PET-PEO multiblock, as reflected by (i) broadening and red-shifting in the 3200–3600 $cm^{-1}$ region and (ii) asymmetry and slight shifts in the carbonyl stretching region. These interactions likely arise from urethane N–H groups interacting with ester and ether functionalities and may contribute to intermolecular association within mixed amorphous regions. These differences can alter the extent to which the hard segment constrains local motion within mixed amorphous regions, thereby affecting the balance between permeability and selectivity. In this context, the butylene-based hard segments of PolyActive may provide more effective confinement of PEO segmental motion than PET, contributing to somewhat greater molecular discrimination, whereas the PET-based system studied here appears to favor higher local mobility and correspondingly modest reductions in selectivity.

Although $CO_2$ plasticization resistance was not directly evaluated in this study, the structural characteristics of these PET–PEO multiblock copolymers suggest behavior intermediate between highly rubbery PEO-rich membranes and rigid glassy aromatic polyesters. Ether-rich PEO segments are expected to enhance $CO_2$ sorption and therefore increase susceptibility to $CO_2$-induced swelling relative to neat PET.[94,95,108] However, DSC results showing suppressed PEO crystallization, together with SAXS evidence for the absence of long-range ordered soft-segment domains, indicate that PEO segments remain structurally constrained within the semicrystalline PET framework.[82–86] These constraints, combined with the rigidifying influence of PET crystalline domains, may mitigate excessive $CO_2$-induced chain mobility relative to physically blended PET/PEO systems. Future high-pressure permeation studies will be required to directly establish plasticization resistance and plasticization pressure in these recycled multiblock membranes.

Taken together, these results demonstrate that membranes derived from recycled consumer PET can achieve $CO_2/CH_4$ separation performance comparable to established virgin PBT–PEO membrane materials, without relying on physical blending strategies that compromise membrane function. While PET–PEO multiblock copolymers do not match PolyActive's selectivity, their performance demonstrates that long-range ordered microphase separation is not required to achieve meaningful transport enhancement. Rather, controlled perturbation of semicrystalline PET morphology through covalent incorporation of PEO provides an effective route for tuning the permeability-selectivity balance in recycled polymer-derived gas separation membranes.

### Extension to polycarbonate-derived multiblock copolymers

While the primary focus of this work is on PET-derived telechelic oligomers, the HDI-mediated coupling strategy should, in principle, be applicable to a broader range of chemically recycled feedstocks. To probe this generality, we performed preliminary experiments using bisphenol-A (BPA) and polycarbonate (PC)-derived oligomers as model telechelic building blocks and coupled them with PEO to form BPA–PEO and PC–PEO multiblock copolymers.

Fig. 7 summarizes these results. Schemes in Fig. 7a and b illustrate the synthetic routes used to prepare BPA–PEO and PC–PEO multiblocks: phenol-terminated BPA or depolymerized PC oligomers are first end-capped with HDI, then reacted with dihydroxy-terminated PEO to generate urethane-linked multiblock architectures. Representative GPC traces (Fig. 7c and d) show that, in both systems, coupling produces clear shifts to lower elution volume relative to the starting PEO and PC/BPA oligomers, indicative of molecular-weight growth upon multiblock formation.

The evolution of molar mass and dispersity with reaction time is quantified in Fig. 7e. For the BPA–PEO system, $M_n$ and $M_w$ increase substantially relative to the 4 kg $mol^{-1}$ PEO precursor, reaching values on the order of ~14 kDa ($M_n$) and ~23 kDa ($M_w$) after extended reaction (19 h), with dispersity narrowing to ~1.6 (Table S6). Similarly, the PC–PEO system shows growth from ~5.0 kDa (PEO) and ~3.2 kDa (dPC) to ~8.0 kDa ($M_n$) and ~15.7 kDa ($M_w$) after 48 h of coupling, accompanied by a broadened $Đ$ characteristic of step-growth assembly from telechelic oligomers (Table S7). The side-by-side comparison in Fig. 7e highlights that both BPA- and PC-based systems undergo efficient chain extension under the same HDI-mediated coupling conditions, despite differences in feedstock structure and initial molar mass.

Time-dependent trends in molecular-weight growth are further emphasized in Fig. 7f, which plots the percent change in $M_n$ and $M_w$ for BPA–PEO and PC–PEO relative to their respective starting oligomers. Both systems exhibit monotonic increases in $M_n$ and $M_w$ with reaction time, consistent with ongoing step-growth coupling rather than simple end-capping. The somewhat larger relative increases observed for BPA–PEO reflect the lower initial molar mass of the early PEO-BPA species (Table S6), whereas the PC–PEO system shows more

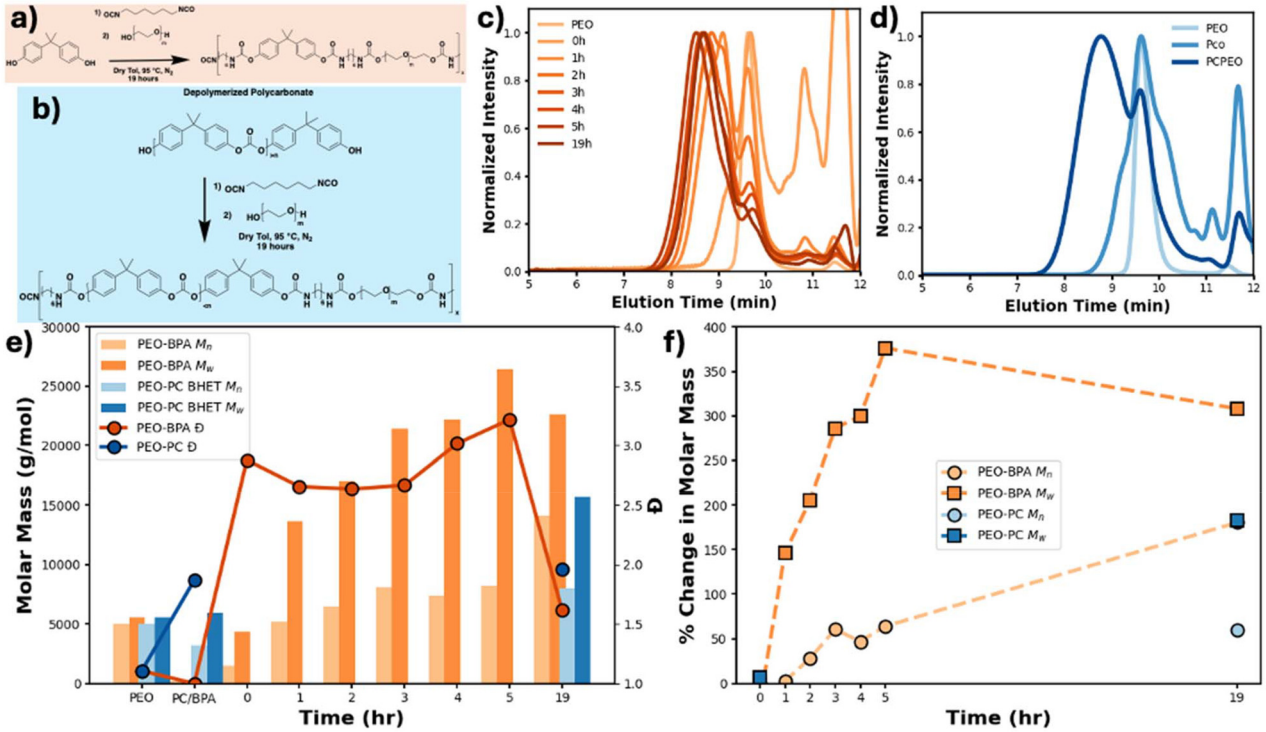


**Fig. 7** Extension of the HDI-mediated multiblock strategy to BPA- and PC-derived oligomers. (a) Synthetic scheme for BPA–PEO multiblock copolymer formation *via* HDI-mediated coupling. (b) Synthetic scheme for PC–PEO multiblock copolymer formation using depolymerized, phenol-terminated PC oligomers and PEO. (c) Representative GPC traces for BPA–PEO samples, showing molecular-weight growth relative to the starting PEO and BPA-derived oligomers. (d) Representative GPC traces for PC–PEO samples, showing molecular-weight growth relative to the starting PEO and depolymerized PC (dPC). (e) Number-average molar mass ($M_n$, light orange for BPA-PEO; light blue for PC–PEO), weight-average molar mass ($M_w$, orange for BPA–PEO; blue for PC–PEO), and dispersity $Đ$ (lines; orange for BPA–PEO, blue for PC–PEO) for the final multiblock products. (f) Percent change in $M_n$ (circles) and $M_w$ (squares) relative to the corresponding starting oligomers for BPA–PEO (orange) and PC–PEO (blue), illustrating time-dependent molecular-weight growth consistent with step-growth multiblock formation.

modest, but still significant, increases in $M_n$ and $M_w$ from the dPC/PEO starting point (Table S7). In both cases, the combination of substantial molecular-weight growth and controlled, step-growth-like dispersities indicates that telechelic oligomers are successfully assembled into multiblock architectures using the same HDI-mediated chemistry developed for PET.

Complementary spectroscopic data (Fig. S24–S26) support this interpretation. FTIR spectra show the disappearance of isocyanate stretching bands and the growth of urethane carbonyl and N–H absorptions as the reactions proceed, while DOSY NMR of the PC–PEO product (Fig. S26) reveals that PEO- and PC-derived resonances share a common diffusion coefficient distinct from those of the corresponding precursors, confirming covalent incorporation of both segments into a single diffusing macromolecular species.

Taken together, the BPA–PEO and PC–PEO results in Fig. 7 demonstrate that telechelic oligomers obtained from different commodity polymers (PET and PC) can be intercepted and recombined using a unified HDI-mediated coupling strategy to form multiblock copolymers with increased molar mass and verified block connectivity. Although a full investigation of the structure–property relationships in these PC-based multiblocks is beyond the scope of this initial study, these experiments underscore the modularity and generality of using waste-derived telechelic oligomers as programmable building blocks for multiblock synthesis.

## Conclusion

This work demonstrates a versatile upcycling strategy that converts depolymerized PET oligomers into high-molecular-weight PET–PEO multiblock copolymers by intercepting telechelic oligomers and coupling them *via* HDI-mediated urethane chemistry. By directly isolating and utilizing telechelic intermediates from depolymerized consumer PET, this approach eliminates the need to revert to monomeric feedstocks, providing a new pathway for transforming waste polymers into architecturally complex materials. Model BHET and PEO systems show that HDI remains reactive over extended periods, indicating that end-capping conditions can unintentionally promote oligomer–oligomer coupling. We show that the timing of the end-capping step governs the competition between chain extension and termination, establishing end-capping time as a critical and previously underexplored control parameter for programming multiblock architecture. Translating this insight to depo-

lymerized PET shows that HDI end-capping time is a powerful synthetic handle: short end-capping suppresses PET–PET self-coupling and enables near-stoichiometric PET–PEO incorporation, whereas extended end-capping produces PET-enriched multiblocks with longer hard segments.

Beyond PET–PEO, this chemistry provides a general platform to construct multiblock copolymers from diverse depolymerization products. Preliminary extension of the HDI-mediated coupling strategy to polycarbonate-derived oligomers (Fig. 7) demonstrates that well-defined telechelic oligomers obtained from chemical recycling can be recombined with PEO to form new multiblock architectures with increased molar mass and characteristic step-growth dispersities. More broadly, these results suggest that phenol- or hydroxyl-terminated carbonate and ester oligomers derived from chemical recycling can serve as modular, reactive building blocks rather than merely intermediates *en route* to monomer recovery. Ongoing and future efforts will extend this approach to additional recycled feedstocks (*e.g.*, textiles such as nylon and PET, and polyethylene-derived diols), enabling systematic control over block composition, sequence length, and phase behavior, and establishing a modular route to value-added upcycled materials directly from plastic waste.

The resulting control over the molecular sequence distribution and connectivity of the copolymer directly governs macroscopic mechanical, swelling, and gas-transport properties. PET–PEO multiblocks balance high strength and ductility more effectively than physical PET/PEO blends (compatibilized or uncompatibilized) or repolymerized PET alone, while their accessible PEO-rich domains dramatically increase water uptake and gas permeability. While these materials do not outperform state-of-the-art PBT–PEO (poly(ether–ester)) membrane systems, they represent, to our knowledge, the first demonstration of PET–PEO multiblock copolymers derived from post-consumer PET for gas transport applications. Importantly, the covalent multiblock molecular connectivity enhances permeability without sacrificing selectivity, approaching the performance of commercial poly(ether–ester) membranes and surpassing compatibilized blends at comparable compositions. Preliminary extension of this chemistry to PEO–PC systems underscore its generality, suggesting a modular platform for constructing multiblock copolymers from diverse depolymerized feedstocks. Overall, this work establishes telechelic oligomers derived from plastic waste as tunable, programmable building blocks for multiblock polymer synthesis and demonstrates a generalizable strategy for converting consumer waste into functional materials without requiring complete depolymerization to monomers. By introducing end-capping time as a design parameter for controlling multiblock architecture, this approach provides a new framework for engineering structure–property relationships in upcycled polymer systems.

We note that the PET–PEO multiblock copolymers reported here do not constitute a fully closed-loop recycling solution. Rather, this chemistry is intended as an upcycling route that broadens the set of materials accessible from chemically recycled PET by converting telechelic oligomers into higher-value, functional architectures. As such, the resulting multiblock copolymers will themselves require appropriate end-of-life management, and future work will be needed to design upcycled systems with intentionally programmable recyclability and to evaluate their environmental performance *via* life-cycle assessment. Nevertheless, by transforming a portion of post-consumer PET into mechanically robust, membrane-relevant materials, this approach has the potential to reduce reliance on virgin feedstocks and divert PET from short-lived, single-use applications that are most prone to environmental release.

## Author contributions

S. W.-S. contributed to conceptualization, investigation, methodology, and writing – original draft. A. B. contributed to the methodology. K. G. contributed to the investigation. N. J. G. contributed to investigation and writing – review & editing. T. S. contributed resources. B. K. L. contributed to writing – review & editing. M. D. D. contributed to project administration, methodology, funding acquisition, and writing – review & editing. All authors meet the journal's authorship criteria, have approved the final version of the manuscript, and agree to be accountable for all aspects of the work.

## Conflicts of interest

We, the authors, have a patent application related to the work presented in this manuscript.

## Data availability

The data supporting the findings of this study are available within the article and its supplementary information (SI). Supplementary information: experimental methods; NMR ($^1$H and DOSY), DSC, and FTIR characterization data; molecular weight analyses (including absolute molecular weight determination and Mark–Houwink analysis); swelling measurements; mechanical testing; gas permeation; polycarbonate depolymerization and upcycling. See DOI: https://doi.org/10.1039/d6gc01907b.

## Acknowledgements

This work was supported by the National Science Foundation, Polymers program, Division of Materials Research (DMR-2104982). The SEC analysis and some of the mechanistic discussions were supported by the US Department of Energy, Office of Science, Materials Sciences and Engineering Division.

## References


1 N. George and T. Kurian, Recent Developments in the Chemical Recycling of Postconsumer Poly(ethylene terephthalate) Waste, *Ind. Eng. Chem. Res.*, 2014, **53**(37), 14185–14198, DOI: 10.1021/ie501995m.

2 B. Fox, G. Moad, G. Van Diepen, I. Willing and W. D. Cook, Characterization of poly(ethylene terephthalate) and poly(ethylene terephthalate) blends, *Polymer*, 1997, **38**(12), 3035–3043, DOI: 10.1016/s0032-3861(96)00872-5.

3 Agency, U. S. E. P., *Facts and Figures about Materials, Waste and Recycling*, ed. Agency, U. S. E. P., 2023.

4 M. Arifuzzaman, B. G. Sumpter, Z. Demchuk, C. Do, M. A. Arnould, M. A. Rahman, P.-F. Cao, I. Popovs, R. J. Davis, S. Dai and T. Saito, Selective deconstruction of mixed plastics by a tailored organocatalyst, *Mater. Horiz.*, 2023, **10**(9), 3360–3368, DOI: 10.1039/d3mh00801k.

5 P. G. C. Nayanathara Thathsarani Pilapitiya and A. S. Ratnayake, The world of plastic waste: A review, *Cleaner Mater.*, 2024, **11**, 100220, DOI: 10.1016/j.clema.2024.100220.

6 L. Lebreton and A. Andrady, Future scenarios of global plastic waste generation and disposal, *Palgrave Commun.*, 2019, **5**(1), 1–11, DOI: 10.1057/s41599-018-0212-7.

7 M. G. Kibria, N. I. Masuk, R. Safayet, H. Q. Nguyen and M. Mourshed, Plastic Waste: Challenges and Opportunities to Mitigate Pollution and Effective Management, *Int. J. Environ. Res.*, 2023, **17**(1), 20, DOI: 10.1007/s41742-023-00507-z.

8 A. E. Schwarz, S. M. C. Lensen, E. Langeveld, L. A. Parker and J. H. Urbanus, Plastics in the global environment assessed through material flow analysis, degradation and environmental transportation, *Sci. Total Environ.*, 2023, **875**, 162644, DOI: 10.1016/j.scitotenv.2023.162644.

9 A. Gómez-Sanabria and F. Lindl, The crucial role of circular waste management systems in cutting waste leakage into aquatic environments, *Nat. Commun.*, 2024, **15**(1), 5443, DOI: 10.1038/s41467-024-49555-9.

10 L. Su, X. Xiong, Y. Zhang, C. Wu, X. Xu, C. Sun and H. Shi, Global transportation of plastics and microplastics: A critical review of pathways and influences, *Sci. Total Environ.*, 2022, **831**, 154884, DOI: 10.1016/j.scitotenv.2022.154884.

11 K. Ziani, C.-B. Ioniță-Mîndrican, M. Mititelu, S. M. Neacșu, C. Negrei, E. Moroșan, D. Drăgănescu and O.-T. Preda, Microplastics: A Real Global Threat for Environment and Food Safety: A State of the Art Review, *Nutrients*, 2023, **15**(3), 617, DOI: 10.3390/nu15030617.

12 S. Allen, D. Allen, S. Karbalaei, V. Maselli and T. R. Walker, Micro(nano)plastics sources, fate, and effects: What we know after ten years of research, *J. Hazard. Mater. Adv.*, 2022, **6**, 100057, DOI: 10.1016/j.hazadv.2022.100057.

13 P. Stegmann, V. Daioglou, M. Londo, D. P. Van Vuuren and M. Junginger, Plastic futures and their CO2 emissions, *Nature*, 2022, **612**(7939), 272–276, DOI: 10.1038/s41586-022-05422-5.

14 V. Sinha, M. R. Patel and J. V. Patel, PET waste management by chemical recycling: a review, *J. Polym. Environ.*, 2010, **18**(1), 8–25.

15 C. Jehanno, I. Flores, A. P. Dove, A. J. Müller, F. Ruipérez and H. Sardon, Organocatalysed depolymerisation of PET in a fully sustainable cycle using thermally stable protic ionic salt, *Green Chem.*, 2018, **20**(6), 1205–1212, DOI: 10.1039/c7gc03396f.

16 D. Carta, G. Cao and C. D'Angeli, Chemical recycling of poly(ethylene terephthalate) (pet) by hydrolysis and glycolysis, *Environ. Sci. Pollut. Res.*, 2003, **10**(6), 390–394, DOI: 10.1065/espr2001.12.104.8.

17 J. H. Clark, J. A. Alonso, J. A. Villalba, J. Aguado, D. P. Serrano and D. Serrano, *Feedstock recycling of plastic wastes*, Royal society of chemistry, 1999.

18 A. J. Zervoudakis, C. S. Sample, X. Peng, D. Lake, M. A. Hillmyer and C. J. Ellison, Dihydroxy Polyethylene Additives for Compatibilization and Mechanical Recycling of Polyethylene Terephthalate/Polyethylene Mixed Plastic Waste, *ACS Macro Lett.*, 2022, 1396–1402, DOI: 10.1021/acsmacrolett.2c00601.

19 K. Nomura, X. Peng, H. Kim, K. Jin, H. J. Kim, A. F. Bratton, C. R. Bond, A. E. Broman, K. M. Miller and C. J. Ellison, Multiblock Copolymers for Recycling Polyethylene-Poly(ethylene terephthalate) Mixed Waste, *ACS Appl. Mater. Interfaces*, 2020, **12**(8), 9726–9735, DOI: 10.1021/acsami.9b20242.

20 J. Xu, J. M. Eagan, S.-S. Kim, S. Pan, B. Lee, K. Klimovica, K. Jin, T.-W. Lin, M. J. Howard, C. J. Ellison, A. M. Lapointe, G. W. Coates and F. S. Bates, Compatibilization of Isotactic Polypropylene (*i*-PP) and High-Density Polyethylene (HDPE) with *i*-PP-PE Multiblock Copolymers, *Macromolecules*, 2018, **51**(21), 8585–8596, DOI: 10.1021/acs.macromol.8b01907.

21 S. M. Al-Salem, P. Lettieri and J. Baeyens, Recycling and recovery routes of plastic solid waste (PSW): A review, *Waste Manage.*, 2009, **29**(10), 2625–2643, DOI: 10.1016/j.wasman.2009.06.004.

22 J. Mata-Alvarez, S. Macé and P. Llabrés, Anaerobic digestion of organic solid wastes. An overview of research achievements and perspectives, *Bioresour. Technol.*, 2000, **74**(1), 3–16, DOI: 10.1016/s0960-8524(00)00023-7.

23 A. Karmakar, T. Daftari, K. Sivagami, A. H. Shaik, B. Kiran and S. Chakraborty, A comprehensive insight into Waste to Energy conversion strategies in India and its associated air pollution hazard, *Environ. Technol. Innovation*, 2023, **29**, 103017, DOI: 10.1016/j.eti.2023.103017.

24 M. Beikmohammadi, K. Yaghmaeian, R. Nabizadeh and A. H. Mahvi, Analysis of heavy metal, rare, precious, and metallic element content in bottom ash from municipal solid waste incineration in Tehran based on particle size, *Sci. Rep.*, 2023, **13**(1), 16044, DOI: 10.1038/s41598-023-43139-1.

25 T. F. Astrup, D. Tonini, R. Turconi and A. Boldrin, Life cycle assessment of thermal Waste-to-Energy techno-

logies: Review and recommendations, *Waste Manage.*, 2015, **37**, 104–115, DOI: 10.1016/j.wasman.2014.06.011.

26 J. Dong, Y. Tang, A. Nzihou, Y. Chi, E. Weiss-Hortala, M. Ni and Z. Zhou, Comparison of waste-to-energy technologies of gasification and incineration using life cycle assessment: Case studies in Finland, France and China, *J. Cleaner Prod.*, 2018, **203**, 287–300, DOI: 10.1016/j.jclepro.2018.08.139.

27 C. S. Psomopoulos, A. Bourka and N. J. Themelis, Waste-to-energy: A review of the status and benefits in USA, *Waste Manage.*, 2009, **29**(5), 1718–1724, DOI: 10.1016/j.wasman.2008.11.020.

28 I. S. Antonopoulos, G. Perkoulidis, D. Logothetis and C. Karkanias, Ranking municipal solid waste treatment alternatives considering sustainability criteria using the analytical hierarchical process tool, *Resour., Conserv. Recycl.*, 2014, **86**, 149–159, DOI: 10.1016/j.resconrec.2014.03.002.

29 S. S. V. Vuppaladadiyam, A. K. Vuppaladadiyam, A. Sahoo, A. Urgunde, S. Murugavelh, V. Šrámek, M. Pohořelý, L. Trakal, S. Bhattacharya, A. K. Sarmah, K. Shah and K. K. Pant, Waste to energy: Trending key challenges and current technologies in waste plastic management, *Sci. Total Environ.*, 2024, **913**, 169436, DOI: 10.1016/j.scitotenv.2023.169436.

30 S. Watson-Sanders and M. Dadmun, More Efficient Chemical Recycling of Poly(Ethylene Terephthalate) by Intercepting Intermediates, *ChemSusChem*, 2024, **17**(23), e202301698, DOI: 10.1002/cssc.202301698.

31 T. Yang, Z. Yang, Y. Zhang, C. Hu, Z. Xie, Z. Sun, X. Pang and X. Chen, Upcycling of PET waste: from one polymer to another polymer, *Polym. Chem.*, 2026, **17**, 7–20, DOI: 10.1039/d5py00861a.

32 Z. Jia, L. Gao, L. Qin and J. Yin, Chemical recycling of PET to value-added products, *RSC Sustain.*, 2023, **1**(9), 2135–2147, DOI: 10.1039/d3su00311f.

33 Y. Peng, Y. Wang, L. Ke, L. Dai, Q. Wu, K. Cobb, Y. Zeng, R. Zou, Y. Liu and R. Ruan, A review on catalytic pyrolysis of plastic wastes to high-value products, *Energy Convers. Manage.*, 2022, **254**, 115243, DOI: 10.1016/j.enconman.2022.115243.

34 X. Wang, J. Xu, M. Zhao, W. Cui, X. Mu, X. Wang, S. Song and H. Zhang, Recent progress of waste plastic upcycling based on multifunctional zeolite catalysts, *Chem. Synth.*, 2024, **4**(2), 67, DOI: 10.20517/cs.2023.67.

35 M. Chu, Q. Kang, P. Hu, Q. Zhang and J. Chen, Unlocking opportunities: Supported metal catalysts for the chemical upcycling of waste plastics, *Chem. Eng. J.*, 2024, **496**, 154375, DOI: 10.1016/j.cej.2024.154375.

36 O. Guselnikova, O. Semyonov, E. Sviridova, R. Gulyaev, A. Gorbunova, D. Kogolev, A. Trelin, Y. Yamauchi, R. Boukherroub and P. Postnikov, "Functional upcycling" of polymer waste towards the design of new materials, *Chem. Soc. Rev.*, 2023, **52**(14), 4755–4832, DOI: 10.1039/d2cs00689h.

37 R. Balu, N. K. Dutta and N. Roy Choudhury, Plastic, Waste Upcycling: A Sustainable Solution for Waste Management, Product Development, and Circular Economy, *Polymers*, 2022, **14**(22), 4788, DOI: 10.3390/polym14224788.

38 D. Sajwan, A. Sharma, M. Sharma and V. Krishnan, Upcycling of Plastic Waste Using Photo-, Electro-, and Photoelectrocatalytic Approaches: A Way toward Circular Economy, *ACS Catal.*, 2024, **14**(7), 4865–4926, DOI: 10.1021/acscatal.4c00290.

39 S. Sun and W. Huang, Chemical Upcycling of Polyolefin Plastics Using Structurally Well-defined Catalysts, *JACS Au*, 2024, **4**(6), 2081–2098, DOI: 10.1021/jacsau.4c00289.

40 S. Kim, D. Kong, X. Zheng and J. H. Park, Upcycling plastic wastes into value-added products via electrocatalysis and photoelectrocatalysis, *J. Energy Chem.*, 2024, **91**, 522–541, DOI: 10.1016/j.jechem.2024.01.010.

41 M. Jiang, X. Wang, W. Xi, P. Yang, H. Zhou, J. Duan, M. Ratova and D. Wu, Chemical catalytic upgrading of polyethylene terephthalate plastic waste into value-added materials, fuels and chemicals, *Sci. Total Environ.*, 2024, **912**, 169342, DOI: 10.1016/j.scitotenv.2023.169342.

42 W. Zimmermann, Biocatalytic recycling of polyethylene terephthalate plastic, *Philos. Trans. R. Soc., A*, 2020, **378**(2176), 20190273, DOI: 10.1098/rsta.2019.0273.

43 J. Mudondo, H.-S. Lee, Y. Jeong, T. H. Kim, S. Kim, B. H. Sung, S.-H. Park, K. Park, H. G. Cha, Y. J. Yeon and H. T. Kim, Recent Advances in the Chemobiological Upcycling of Polyethylene Terephthalate (PET) into Value-Added Chemicals, *J. Microbiol. Biotechnol.*, 2023, **33**(1), 1–14, DOI: 10.4014/jmb.2208.08048.

44 X. Zhang, H. Yang, Z. Chen, X. Wang, H. Feng, J. Zhang, J. Yu, S. Gao and D. Lai, Sustainable production of aromatics via catalytic pyrolysis of polyolefins towards the carbon cycle for plastics, *Fuel*, 2024, **357**, 129897, DOI: 10.1016/j.fuel.2023.129897.

45 L. Fu, Q. Xiong, Q. Wang, L. Cai, Z. Chen and Y. Zhou, Catalytic Pyrolysis of Waste Polyethylene Using Combined CaO and Ga/ZSM-5 Catalysts for High Value-Added Aromatics Production, *ACS Sustainable Chem. Eng.*, 2022, **10**(29), 9612–9623, DOI: 10.1021/acssuschemeng.2c02881.

46 D. B. Tiz, F. A. Vicente, A. Kroflič and B. Likozar, Lignin-Based Covalent Adaptable Network Polymers–When Bio-Based Thermosets Meet Recyclable by Design, *ACS Sustainable Chem. Eng.*, 2023, **11**(38), 13836–13867, DOI: 10.1021/acssuschemeng.3c03248.

47 M. K. Danielson, C. Gainaru, Z. Demchuk, C. Pan, J. Choi, H. H. Zhang, J. C. Foster, T. Saito and M. A. Rahman, Closed-Loop Recyclable Vitrimer Plastics from PET Waste: A Design for Circularity, *ChemSusChem*, 2025, **18**(18), e202500898, DOI: 10.1002/cssc.202500898.

48 S. R. Watson-Sanders, K. D. Johnson, T. Taylor, S. Barber and M. D. Dadmun, Energy-Efficient Upcycling of Waste Poly(ethylene terephthalate) via Pre-Annealing-Induced Formation of Reactive Telechelic Oligomers, *ACS Sustainable Chem. Eng.*, 2026, **14**(13), 6319–6329, DOI: 10.1021/acssuschemeng.5c12510.

49 C. Paul and T. P. L. Hiemenz, *Polymer Chemistry*, CRC Press, 2007.

50 J. Roovers and P. M. Toporowski, Hydrodynamic studies on model branched polystyrenes, *J. Polym. Sci., Polym. Phys. Ed.*, 1980, **18**(9), 1907–1917, DOI: 10.1002/pol.1980.180180904.
51 Y. Liu, L. Yin, H. Zhao, G. Song, F. Tang, L. Wang, H. Shao and Y. Zhang, Lamellar and fibrillar structure evolution of poly(ethylene terephthalate) fiber in thermal annealing, *Polymer*, 2016, **105**, 157–166, DOI: 10.1016/j.polymer.2016.10.031.
52 Z. Chen, M. J. Jenkins and J. N. Hay, Annealing of poly (ethylene terephthalate), *Eur. Polym. J.*, 2014, **50**, 235–242, DOI: 10.1016/j.eurpolymj.2013.11.004.
53 P. J. Holdsworth and A. Turner-Jones, The melting behaviour of heat crystallized poly(ethylene terephthalate), *Polymer*, 1971, **12**(3), 195–208, DOI: 10.1016/0032-3861(71)90045-0.
54 R. L. Blaine, Determination of Polymer Crystallinity by DSC, TA Instruments, https://www.tainstruments.com/pdf/literature/TA123new.pdf (accessed 2023 07/14/23).
55 R. L. Blaine, Thermal Applications Note, TA Instrument, https://www.tainstruments.com/pdf/literature/TN048.pdf (accessed 2023 07/14/23).
56 A. Wallard, *Measurement Principles and Structures*, Springer Berlin Heidelberg, 2006, pp. 3–16.
57 D. J. Fortman, D. T. Sheppard and W. R. Dichtel, Reprocessing Cross-Linked Polyurethanes by Catalyzing Carbamate Exchange, *Macromolecules*, 2019, **52**(16), 6330–6335, DOI: 10.1021/acs.macromol.9b01134.
58 J. L. Swartz, D. T. Sheppard, G. Haugstad and W. R. Dichtel, Blending Polyurethane Thermosets Using Dynamic Urethane Exchange, *Macromolecules*, 2021, **54**(23), 11126–11133, DOI: 10.1021/acs.macromol.1c01910.
59 C. Bakkali-Hassani, D. Berne, V. Ladmiral and S. Caillol, Transcarbamoylation in Polyurethanes: Underestimated Exchange Reactions?, *Macromolecules*, 2022, **55**(18), 7974–7991, DOI: 10.1021/acs.macromol.2c01184.
60 M. I. Aranguren and R. J. J. Williams, Kinetic and statistical aspects of the formation of polyurethanes from toluene diisocyanate, *Polymer*, 1986, **27**(3), 425–430, DOI: 10.1016/0032-3861(86)90160-6.
61 F. Schmitt, A. Wenning and J.-V. Weiss, Dimeric isocyanates in polyurethane powder coatings, *Prog. Org. Coat.*, 1998, **34**(1–4), 227–235, DOI: 10.1016/s0300-9440(98)00036-8.
62 C. Zavarise, J.-C. Cintrat, E. Romero and A. Sallustrau, Isocyanate-based multicomponent reactions, *RSC Adv.*, 2024, **14**(53), 39253–39267, DOI: 10.1039/d4ra04152f.
63 T. Nagy, B. Antal, K. Czifrák, I. Papp, J. Karger-Kocsis, M. Zsuga and S. Kéki, New insight into the kinetics of diisocyanate-alcohol reactions by high-performance liquid chromatography and mass spectrometry, *J. Appl. Polym. Sci.*, 2015, **132**(25), 42127, DOI: 10.1002/app.42127.
64 O. Welz, M. Pfeifle, P. M. Plehiers, R. Sure and P. Deglmann, Reaction of OH with Aliphatic and Aromatic Isocyanates, *J. Phys. Chem. A*, 2022, **126**(50), 9333–9352, DOI: 10.1021/acs.jpca.2c06011.
65 B. Grepinet, F. Pla, P. Hobbes, T. Monge and P. Swaels, Modeling and simulation of urethane acrylates synthesis. II. Kinetics of uncatalyzed reaction of toluene diisocyanate with a polyether diol, *J. Appl. Polym. Sci.*, 2001, **81**(13), 3149–3160, DOI: 10.1002/app.1767.
66 Z. Wang, Y. Zhao and Y. Wei, Syntheses and properties of tri- and multi-block copolymers consisting of polybutadiene and polylactide segments, *RSC Adv.*, 2022, **12**(46), 29777–29784, DOI: 10.1039/d2ra05051j.
67 M. Behl, M. Balk, K. Lützow and A. Lendlein, Impact of block sequence on the phase morphology of multiblock copolymers obtained by high-throughput robotic synthesis, *Eur. Polym. J.*, 2021, **143**, 110207, DOI: 10.1016/j.eurpolymj.2020.110207.
68 E. Galanos, E. Grune, C. Wahlen, A. H. E. Müller, M. Appold, M. Gallei, H. Frey and G. Floudas, Tapered Multiblock Copolymers Based on Isoprene and 4-Methylstyrene: Influence of the Tapered Interface on the Self-Assembly and Thermomechanical Properties, *Macromolecules*, 2019, **52**(4), 1577–1588, DOI: 10.1021/acs.macromol.8b02669.
69 G. P. Baeza, Recent advances on the structure-properties relationship of multiblock copolymers, *J. Polym. Sci.*, 2021, **59**(21), 2405–2433, DOI: 10.1002/pol.20210406.
70 R. J. Gaymans, Segmented copolymers with monodisperse crystallizable hard segments: Novel semi-crystalline materials, *Prog. Polym. Sci.*, 2011, **36**(6), 713–748, DOI: 10.1016/j.progpolymsci.2010.07.012.
71 I. Yilgör, E. Yilgör and G. L. Wilkes, Critical parameters in designing segmented polyurethanes and their effect on morphology and properties: A comprehensive review, *Polymer*, 2015, **58**, A1–A36, DOI: 10.1016/j.polymer.2014.12.014.
72 A. Arun, K. Dullaert and R. J. Gaymans, Structure and Properties of Mono-, Di-, Tri- and Multiblock Segmented Copolymers with Diamide Hard Segments, *Macromol. Chem. Phys.*, 2009, **210**(1), 48–59, DOI: 10.1002/macp.200800406.
73 Z. Genene, J. W. Lee, S. W. Lee, Q. Chen, Z. Tan, B. A. Abdulahi, D. Yu, T. S. Kim, B. J. Kim and E. Wang, Polymer Acceptors with Flexible Spacers Afford Efficient and Mechanically Robust All-Polymer Solar Cells, *Adv. Mater.*, 2022, **34**(6), 2107361, DOI: 10.1002/adma.202107361.
74 R. Zhang, Q. He, H. Yu, J. Li, Y. Hu and J. Qian, Impact of Hexyl Branch Content on the Mechanical Properties and Deformation Mechanisms of Amorphous Ethylene/1-Octene Copolymers: A Molecular Dynamics Study, *Polymers*, 2024, **16**(23), 3236, DOI: 10.3390/polym16233236.
75 F. Sugiyama, A. T. Kleinschmidt, L. V. Kayser, D. Rodriquez, M. Finn, M. A. Alkhadra, J. M. H. Wan, J. Ramírez, A. S. C. Chiang, S. E. Root, S. Savagatrup and D. J. Lipomi, Effects of flexibility and branching of side chains on the mechanical properties of low-bandgap conjugated polymers, *Polym. Chem.*, 2018, **9**(33), 4354–4363, DOI: 10.1039/c8py00820e.

76 Z. Wang, X. Lin, T. Yu, N. Zhou, H. Zhong and J. Zhu, Formation and rupture mechanisms of visco-elastic interfacial films in polymer-stabilized emulsions, *J. Dispersion Sci. Technol.*, 2019, **40**(4), 612–626, DOI: 10.1080/01932691.2018.1478303.

77 M. Matsuda, C.-Y. Lin, K. Enomoto, Y.-C. Lin, W.-C. Chen and T. Higashihara, Impact of the Heteroatoms on Mobility-Stretchability Properties of *n*-Type Semiconducting Polymers with Conjugation Break Spacers, *Macromolecules*, 2023, **56**(6), 2348–2361, DOI: 10.1021/acs.macromol.3c00109.

78 T. Kida, R. Tanaka, T. Shiono, H. Takeshita and K. Tokumitsu, Effect of short-chain branches in high-molecular-weight component on tensile properties of polyethylene solids, *Polymer*, 2024, **298**, 126906, DOI: 10.1016/j.polymer.2024.126906.

79 J. Słonecki, Investigations of the hardness and thermal properties of copoly(ether-ester)s containing segments of different molar masss, *Polymer*, 1990, **31**(8), 1464–1466, DOI: 10.1016/0032-3861(90)90151-n.

80 A. A. Deschamps, D. W. Grijpma and J. Feijen, Poly(ethylene oxide)/poly(butylene terephthalate) segmented block copolymers: the effect of copolymer composition on physical properties and degradation behavior, *Polymer*, 2001, **42**(23), 9335–9345, DOI: 10.1016/s0032-3861(01)00453-0.

81 H. Schmalz, V. Van Guldener, W. Gabriëlse, R. Lange and V. Abetz, Morphology, Surface Structure, and Elastic Properties of PBT-Based Copolyesters with PEO-*b*-PEB-*b*-PEO Triblock Copolymer Soft Segments, *Macromolecules*, 2002, **35**(14), 5491–5499, DOI: 10.1021/ma011995o.

82 C. Kundu and A. K. Dasmahapatra, Effect of block asymmetry on the crystallization of double crystalline diblock copolymers, *J. Chem. Phys.*, 2014, **141**(4), 044902, DOI: 10.1063/1.4889997.

83 A. Cicolella, M. Scoti, G. Talarico, A. J. Müller, R. Di Girolamo and C. De Rosa, Crystallization Kinetics of Crystalline-Crystalline and Crystalline-Amorphous Block Copolymers of Linear Polyethylene and Isotactic Polypropylene, *Macromolecules*, 2024, **57**(18), 8748–8762, DOI: 10.1021/acs.macromol.4c01402.

84 K. Yoshida, Y.-I. Hsu, M. Sugimoto and H. Uyama, Synthesis of poly(lactic acid) multiblock copolymers with improved properties using 3-hydroxybutyrate diol, *Polym. Degrad. Stab.*, 2025, **241**, 111570, DOI: 10.1016/j.polymdegradstab.2025.111570.

85 Y. Zhang and W. Zhang, Coarse-Grained Simulations of Crystallization in Phase-Separated Polymer Blends with Block Copolymer Compatibilizers, *Macromolecules*, 2025, **58**(23), 12871–12881, DOI: 10.1021/acs.macromol.5c01767.

86 C. Kundu and A. K. Dasmahapatra, Crystallization of double crystalline symmetric diblock copolymers, *Polymer*, 2014, **55**(3), 958–969, DOI: 10.1016/j.polymer.2013.12.047.

87 M. W. M. Tan, P. M. Thornton, G. Thangavel, H. Bark, R. Dauskardt and P. S. Lee, Toughening Self-Healing Elastomers with Chain Mobility, *Adv. Sci.*, 2024, (30), 11, DOI: 10.1002/advs.202308154.

88 H. Ono, Y. Kawai, S. Ata, H. Minamikawa, K. Kurihara, S. Tanaka and M. Yoshida, Synthesis of Multiblock Copolymer Composed of Biodegradable Poly(butylene succinate) and Poly(2-pyrrolidone): Impact of Each Block Length on the Mechanical Properties, *Macromol. Rapid Commun.*, 2023, **44**(15), 2300155, DOI: 10.1002/marc.202300155.

89 M. Behl, M. Balk, U. Mansfeld and A. Lendlein, Phase Morphology of Multiblock Copolymers Differing in Sequence of Blocks, *Macromol. Mater. Eng.*, 2021, **306**(3), 2000672, DOI: 10.1002/mame.202000672.

90 H. Jung, T. Earmme and S.-H. Choi, Effect of end-block chain length on rheological properties of ABA triblock copolymer hydrogels, *Korea-Aust. Rheol. J.*, 2021, **33**(2), 123–131, DOI: 10.1007/s13367-021-0011-3.

91 Z. Cai, R. G. M. Badr, L. Hauer, K. Chaudhuri, A. Skabeev, F. Schmid and J. T. Pham, Phase separation dynamics in wetting ridges of polymer surfaces swollen with oils of different viscosities, *Soft Matter*, 2024, **20**(36), 7300–7312, DOI: 10.1039/d4sm00576g.

92 M. Li, H. Lu, M. Pi, H. Zhou, Y. Wang, B. Yan, W. Cui and R. Ran, Water-Induced Phase Separation for Anti-Swelling Hydrogel Adhesives in Underwater Soft Electronics, *Adv. Sci.*, 2023, **10**(32), 2304780, DOI: 10.1002/advs.202304780.

93 G. Zhang, J. Steck, J. Kim, C. H. Ahn and Z. Suo, Hydrogels of arrested phase separation simultaneously achieve high strength and low hysteresis, *Sci. Adv.*, 2023, **9**(26), eadh7742, DOI: 10.1126/sciadv.adh7742.

94 A. Ioannidi, D. Vroulias, J. Kallitsis, T. Ioannides and V. Deimede, Synthesis and characterization of poly(ethylene oxide) based copolymer membranes for efficient gas/vapor separation: Effect of PEO content and chain length, *J. Membr. Sci.*, 2021, **632**, 119353, DOI: 10.1016/j.memsci.2021.119353.

95 A. Tena, A. E. Lozano, L. Palacio, A. Marcos-Fernández, P. Prádanos, J. De Abajo and A. Hernández, Gas separation properties of systems with different amounts of long poly(ethylene oxide) segments for mixtures including carbon dioxide, *Int. J. Greenhouse Gas Control*, 2013, **12**, 146–154, DOI: 10.1016/j.ijggc.2012.10.014.

96 M. Karunakaran, R. Shevate, M. Kumar and K. V. Peinemann, $CO_2$-selective PEO-PBT (PolyActive™)/graphene oxide composite membranes, *Chem. Commun.*, 2015, **51**(75), 14187–14190, DOI: 10.1039/c5cc04999g.

97 A. Car, C. Stropnik, W. Yave and K. V. Peinemann, Tailor-made Polymeric Membranes based on Segmented Block Copolymers for $CO_2$ Separation, *Adv. Funct. Mater.*, 2008, **18**(18), 2815–2823, DOI: 10.1002/adfm.200800436.

98 R. W. Baker, *Membrane Technology and Applications*, 2012, DOI: 10.1002/9781118359686.

99 Y. Yampolskii, Polymeric Gas Separation Membranes, *Macromolecules*, 2012, **45**(8), 3298–3311, DOI: 10.1021/ma300213b.

100 J. H. Sim, W. Hong, T. V. Vu, H. Choi, J. Kim, Y. Lee and Y. Kang, Unlocking Hidden Miscibility: Entropy Diluent Strategy for Incompatible Polymer Blends, *Macromolecules*, 2025, **58**(18), 9682–9691, DOI: 10.1021/acs.macromol.5c01387.

101 N. Panapitiya, S. Wijenayake, D. Nguyen, C. Karunaweera, Y. Huang, K. Balkus, I. Musselman and J. Ferraris, Compatibilized Immiscible Polymer Blends for Gas Separations, *Materials*, 2016, **9**(8), 643, DOI: 10.3390/ma9080643.

102 N. P. Panapitiya, S. N. Wijenayake, D. D. Nguyen, Y. Huang, I. H. Musselman, K. J. Balkus and J. P. Ferraris, Gas Separation Membranes Derived from High-Performance Immiscible Polymer Blends Compatibilized with Small Molecules, *ACS Appl. Mater. Interfaces*, 2015, **7**(33), 18618–18627, DOI: 10.1021/acsami.5b04747.

103 N. J. Galan, I. T. Dishner, B. G. Sumpter, V. Kertesz, N. B. Abdul Rahman, F. Polo-Garzon, Z. Demchuk, T. Saito and J. C. Foster, Upcycling of polyethylene terephthalate to high-value chemicals by carbonate-interchange deconstruction, *Green Chem.*, 2025, **27**(47), 15124–15134, DOI: 10.1039/d5gc03354c.

104 M. M. Rahman, C. Abetz, S. Shishatskiy, J. Martin, A. J. Müller and V. Abetz, $CO_2$ Selective PolyActive Membrane: Thermal Transitions and Gas Permeance as a Function of Thickness, *ACS Appl. Mater. Interfaces*, 2018, **10**(31), 26733–26744, DOI: 10.1021/acsami.8b09259.

105 K. Schuldt, J. Pohlmann, S. Shishatskiy and T. Brinkmann, Applicability of PolyActive™ Thin Film Composite Membranes for CO2 Separation from C2H4 Containing Multi-Component Gas Mixtures at Pressures up to 30 Bar, *Membranes*, 2018, **8**(2), 27, DOI: 10.3390/membranes8020027.

106 V. I. Bondar, B. D. Freeman and I. Pinnau, Gas transport properties of poly(ether-b-amide) segmented block copolymers, *J. Polym. Sci., Part B: Polym. Phys.*, 2000, **38**(15), 2051–2062, DOI: 10.1002/1099-0488(20000801)38:15<2051::aid-polb100>3.0.co;2-d.

107 Y. Yamamoto, H. Hoshina and H. Sato, Differences in Intermolecular Interactions and Flexibility between Poly (ethylene terephthalate) and Poly(butylene terephthalate) Studied by Far-Infrared/Terahertz and Low-Frequency Raman Spectroscopy, *Macromolecules*, 2021, **54**(2), 1052–1062, DOI: 10.1021/acs.macromol.0c02049.

108 S. Bandehali, A. Moghadassi, F. Parvizian, S. M. Hosseini, T. Matsuura and E. Joudaki, Advances in high carbon dioxide separation performance of poly (ethylene oxide)-based membranes, *J. Energy Chem.*, 2020, **46**, 30–52, DOI: 10.1016/j.jechem.2019.10.019.